arXiv:1303.6104v1 [cond-mat.stat-mech] 25 Mar 2013

Critical Casimir forces between homogeneous and chemically striped surfaces

Francesco Parisen Toldin
Institut für Theoretische Physik und Astrophysik,
Universität Würzburg, Am Hubland, D-97074 Würzburg, Germany and
Max-Planck-Institut für Physik komplexer Systeme,
Nöthnitzer Str. 38, D-01187 Dresden, Germany[*]

Matthias Tröndle[†] and S. Dietrich[‡]
Max-Planck-Institut für Intelligente Systeme, Heisenbergstr. 3, D-70569 Stuttgart, Germany and
IV. Institut für Theoretische Physik, Universität Stuttgart,
Pfaffenwaldring 57, D-70569 Stuttgart, Germany

Recent experiments have measured the critical Casimir force acting on a colloid immersed in a binary liquid mixture near its continuous demixing phase transition and exposed to a chemically structured substrate. Motivated by these experiments, we study the critical behavior of a system, which belongs to the Ising universality class, for the film geometry with one planar wall chemically striped, such that there is a laterally alternating adsorption preference for the two species of the binary liquid mixture. For the opposite wall we employ alternatively a homogeneous adsorption preference or homogeneous Dirichlet boundary conditions. By means of mean-field theory, Monte Carlo simulations, and finite-size scaling analysis we determine the critical Casimir force acting on the two parallel walls and its corresponding universal scaling function. We show that in the limit of stripe widths small compared with the film thickness, on the striped surface the system effectively realizes Dirichlet boundary conditions, which generically do not hold for actual fluids. Moreover, the critical Casimir force is found to be attractive or repulsive, depending on the width of the stripes of the chemically patterned surface and on the boundary condition applied to the opposing surface.

PACS numbers: 05.70.Jk, 64.60.an, 68.15.+e, 05.50.+q, 05.10.Ln

I. INTRODUCTION

As an intriguing consequence of their presence, fluctuations of an embedding medium may manifest themselves in terms of effective forces acting on its confining boundaries. The critical Casimir force is such a fluctuation-induced force which arises due to the emergence of long-ranged thermal fluctuations if a fluid close to a second-order phase transition is confined between surfaces. This phenomenon, first predicted by Fisher and de Gennes [1] is the analogue of the Casimir effect in quantum electrodynamics [2]. Reference [3] provides a recent review which illustrates analogies as well as differences between these two effects and guides the reader towards further reviews of the subject and the pertinent original literature.

The dependence of the critical Casimir force on the distance between the confinements and on temperature is characterized by a universal scaling function, which is determined by the bulk and surface universality classes (UC) [4, 5] of the confined system. It is independent of microscopic details of the system, and its form depends only on a few global and general properties, such as the spatial dimension d, the number of components of the order parameter, the shape of the confinement, and the type of boundary conditions (BC) [6–8].

In recent years the critical Casimir effect has attracted numerous experimental [9–17] and even more theoretical investigations. Critical Casimir forces can be inferred indirectly by studying wetting films of fluids close to a critical end point [18, 19]. In this context, ^{4}He wetting films close to the onset of superfluidity [9] and wetting films of classical [10] and quantum [11] binary liquid mixtures have been studied experimentally. Only recently direct measurements of the critical Casimir force have been reported [12–16] by monitoring individual colloidal particles immersed into a binary liquid mixture close to its critical demixing point and exposed to a planar wall.

Not only the strength of critical Casimir forces can be tuned by small temperature changes but even their sign depends on the BC of the confining boundaries. The two interfaces of a ^{4}He film impose a symmetry-preserving Dirichlet BC (denoted by (o)) on the superfluid order-parameter at both sides of the film, which causes attractive critical Casimir forces leading to a thinning of the film near the λ-transition [9, 18, 19]. However, for classical binary liquid mixtures (or simple fluids), surfaces preferentially adsorb one of the two species of the mixture (or the gaseous or the liquid phase of a simple fluid, respectively). This corresponds to symmetry-breaking BC (denoted as $(+)$ or $(-)$ BC) acting on the order parameter which is, e.g., the concentration difference in a binary liquid. Within the theoretical description $(\pm)$ BC are realized by surface fields and the (o) BC by their absence.

---

[*] francesco.parisentoldin@physik.uni-wuerzburg.de
[†] troendle@is.mpg.de
[‡] dietrich@is.mpg.de

The emergence of long-ranged thermal fluctuations close to a second-order phase transition leads to a mesoscopic extent of the adsorption layer close to surfaces with $(\pm)$ BC. Depending on whether the adsorption preferences of the confining surfaces of the fluid are the same $(\pm,\pm)$ or different $(+,-)$, critical Casimir forces acting on them are either attractive $(\pm,\pm)$ or repulsive $(+,-)$ [10, 12, 13, 16]. The critical Casimir force between walls with $(\pm)$ BC is the combined effect of the change of the fluctuation spectrum due to the confinement and the interference of the adsorption layers, which are present even within mean-field theory. The shapes of the adsorption layers themselves are strongly influenced by non-Gaussian fluctuations, i.e., they differ from mean-field predictions. In this sense, the effective forces acting on surfaces which confine a (near-) critical fluid provide a classical analogue of the Casimir effect both in the case of symmetry-breaking and in the case of symmetry-preserving BC.

Early on theoretical investigations of the critical Casimir force used, to a large extent, field-theoretical methods (see, e.g., Ref. [20] for a list of references). Only recently Monte Carlo (MC) simulations have allowed for their quantitatively reliable computation. Early numerical simulations for the critical Casimir force have been employed in Ref. [21] for the film geometry with laterally homogeneous BC. More recently the critical Casimir force has been determined by numerical simulations for the XY UC [22–28], which describes the critical properties of the superfluid phase transition in ^{4}He, as well as the Ising UC [20, 22, 24, 25, 29–34] which describes, inter alia, the experimentally relevant demixing transition in a binary liquid mixture.

Since Casimir forces may affect or empower future devices on the micro- and nano-scale, their modifications due to the presence of nano- or micro-structures on the substrates has been a topic of intense research during the last decade. Recent theoretical and experimental studies of QED Casimir forces (see, e.g., Ref. [35] and references therein) as well as critical Casimir forces [36] for *topologically* structured substrates exhibit remarkable deviations from the corresponding ones for planar walls as well as the occurrence of lateral forces. However, only *chemically* patterned substrates allow for interesting combinations of attractive and repulsive critical Casimir forces so that among the various realizations of the critical Casimir effect, the force in the presence of a chemically patterned substrate has recently attracted particular interest [15, 37].

Experiments with binary liquid mixtures as solvents have been used to study critical Casimir forces acting on dissolved colloids close to a chemically structured substrate [14–16], which creates a laterally varying adsorption preference for both components of the solvent. Such kind of systems have been investigated theoretically for the film geometry within mean-field theory [38], within Gaussian approximation [39], and with MC simulations in a three-dimensional film geometry in the presence of a single chemical step [20]. The critical Casimir force in the presence of a patterned substrate has also been studied in the case of a sphere near a planar wall within the Derjaguin approximation [40, 41]. If the lateral chemical patterns do not consist of stripes with sharp chemical steps between areas of strong but opposite adsorption preferences, one faces spatial regions characterized by surface fields of medium strength. This case has been studied so far only for laterally homogeneous BC in the presence of variable boundary fields. This case gives already rise to interesting crossover phenomena, which have been studied within mean-field theory [42], by exact calculations in two spatial dimensions [43, 44], and with MC simulations [31, 32].

Motivated by the aforementioned experimental results, and based on previous investigations by two of the authors [20], here we present a MC study of a three-dimensional lattice model in the film geometry, representing the Ising UC in the presence of a chemically striped substrate. Moreover, we compare the universal scaling functions of the critical Casimir forces obtained from these MC results with the corresponding mean-field results, which we obtain by generalizing a previous study [38] and which are valid in $d = 4$ spatial dimensions. We employ periodic boundary conditions in the lateral directions and different BC for the two surfaces confining the slab. To this end, we consider a film of thickness L confined along the normal z-direction on one side by a surface at which the order parameter of the fluid exhibits a laterally homogeneous BC which corresponds either to strong adsorption $(+)$ or to the so-called ordinary surface transition (o) [4, 5]. The other side of the film is confined by a surface which is periodically patterned by stripes leading to strong, alternating adsorption preferences corresponding to $(+)$ or $(-)$ BC, respectively, varying along the lateral x-direction.

Here, we focus on stripes of equal width $S_+ = S_- = P/2$ corresponding to half of the period P along the x-direction, so that the important geometrical parameter is given by $\kappa \equiv S_+/L$, which relates the width of the stripes to the film thickness (see Figs. 1 and 2). Within the lattice model this system is realized by either fixing the Ising spins in the upper surface to $+1$ or imposing an open boundary by not fixing them, whereas the lower surface consists of alternating stripes of equal width, where the spins are fixed to $+1$ and -1. The chemical steps separating the stripes are taken to be sharp.

Our results show that in the limit of stripe widths small compared to the film thickness, the lower surface effectively realizes Dirichlet BC. Thus the system reduces for $\kappa \to 0$ to $(+,o)$ or (o,o) BC, and, in order to be able to compare with this limiting case, here we also consider a film in which both surfaces have a laterally homogeneous BC from the outset (see Figs. 3 and 4). This may provide a novel possibility of studying also symmetry-preserving BC for simple fluids and binary liquid mixtures which are difficult to establish experimentally otherwise [16].

In order to extract universal quantities from MC simu-

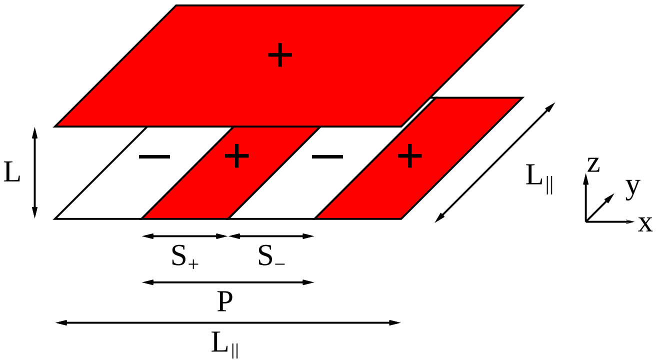

FIG. 1. Film geometry confined by a laterally homogeneous upper surface and by a lower surface with alternating stripes of equal width. At both surfaces the spins are fixed. We choose $S_+ = S_-$ so that the period $P = S_+ + S_- = 2S_+$.

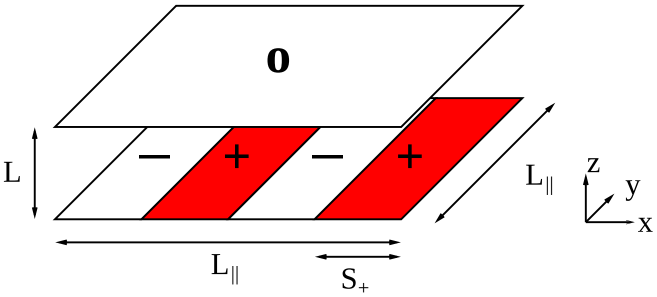

FIG. 2. Film geometry confined by an upper surface with open BC and by a lower surface with alternating stripes of equal width with fixed spins.

lations, it is important to take corrections to scaling into account in order to be able to extrapolate data for systems of finite size L to the thermodynamic limit $L \to \infty$. In particular, in the standard three-dimensional Ising model, scaling corrections are proportional to $L^{-\omega}$, with $\omega = 0.832(6)$ [45]. The presence of non-periodic boundary conditions, such as in the direction normal to the film, gives rise to additional scaling corrections, the leading one being proportional to L^{-1}, which is numerically difficult to disentangle from the previous one. Following Refs. [20, 26, 27, 29, 31], in order to avoid the simultaneous presence of these competing corrections, we have studied a so-called improved model [46], for which the leading scaling corrections $\propto L^{-\omega}$ are suppressed for all observables so that the correction $\propto L^{-1}$ becomes the leading one.

This paper is organized such that in Sec. II the finite-size scaling behavior, as expected for the system under study, is established. In Sec. III we introduce the lattice model studied here. In Secs. IV and V we present our MC results for the critical Casimir force at $T = T_c$ and for the universal scaling function of the critical Casimir force at $T \neq T_c$, respectively. The corresponding results obtained within mean-field theory ($d = 4$) are presented in

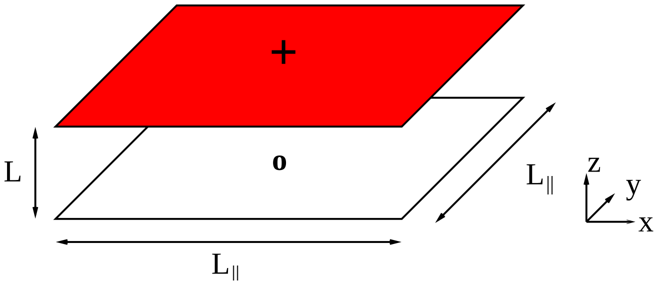

FIG. 3. Film geometry confined by a laterally homogeneous upper surface with fixed spins and by a lower surface with open BC.

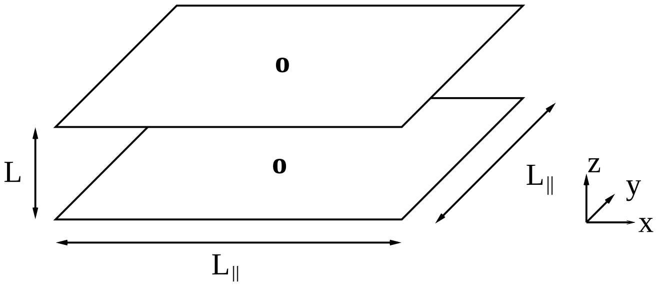

FIG. 4. Film geometry confined by a lower and an upper surface both with open BC.

Sec. VI and compared with the actual behavior in $d = 3$ in Sec. VII. We summarize our main findings in Sec. VIII. In App. A we provide certain important technical details of the MC simulations. In App. B we report details of the determination of the bulk free energy density which is needed in order to compute the critical Casimir force.

II. FINITE-SIZE SCALING AND CRITICAL CASIMIR FORCE

In this section we recall the finite-size scaling (FSS) behavior of a system in the film geometry $L \times L_\|^{d-1}$ in d spatial dimensions, which in the thermodynamic limit exhibits a second-order phase transition at the temperature $T = T_c$. Here, we restrict ourselves to the BC described above; a broader discussion of finite-size scaling for non-periodic BC can be found in Ref. [20]. In the following, for the sake of brevity, we do not analyze separately the FSS behavior of the BC illustrated in Figs. 3 and 4, where there are no stripes. These two cases can be obtained by taking the limit $\kappa = S_+/L \to 0$ in the BC of Figs. 1 and 2, respectively.

In the critical region and in the absence of an external bulk field, the free energy density $\mathcal{F}$ per k_BT of the system (i.e., the free energy divided by $LL_\|^{d-1}k_BT$) can be decomposed into a *s*ingular contribution and a *n*on-singular background term:

$$\mathcal{F}(t,L,L_\|,S_+) = \mathcal{F}^{(\mathrm{s})}(t,L,L_\|,S_+) + \mathcal{F}^{(\mathrm{ns})}(t,L,L_\|,S_+), \tag{1}$$

where $t \equiv (T-T_c)/T_c$ is the reduced temperature. The non-singular background $\mathcal{F}^{(\mathrm{ns})}$ can be further decomposed into specific geometric contributions, corresponding to bulk, surface, and line contributions. According to renormalization-group (RG) theory [47] and neglecting corrections to scaling, in spatial dimension d the singular part of the free energy density obeys the following scaling property:

$$\begin{aligned}\mathcal{F}^{(\mathrm{s})}(t,L,L_\|,S_+) &= \tfrac{1}{L^d} f(\tau,\kappa,\rho),\\ \tau &\equiv t\left(L/\xi_0^+\right)^{1/\nu},\\ \kappa &\equiv S_+/L,\\ \rho &\equiv L/L_\|,\end{aligned} \tag{2}$$

where ν is the critical exponent of the bulk correlation length and ξ_0^+ is its non-universal amplitude:

$$\xi(t\to 0^\pm) = \xi_0^\pm |t|^{-\nu}. \tag{3}$$

The function $f(\tau,\kappa,\rho)$ is a universal scaling function, i.e., it depends only on the bulk universality class and on the BC applied at the two surfaces. As in Ref. [38], the scaling ansatz in Eq. (2) generalizes the one for laterally homogeneous BC by an additional dependence on the scaling variable κ. In the following we neglect the dependence on the aspect ratio $\rho \equiv L/L_\|$ because here we are interested in the film geometry with $L_\| \gg L$. In this limit and for the BC considered here, the dependence on the aspect ratio is expected to be negligible. Our MC data support this observation (see also the discussion in Sec. IV below). The bulk free energy density $f_{\mathrm{bulk}}(t)$ is defined as

$$f_{\mathrm{bulk}}(t) \equiv \lim_{L,L_\|\to\infty} \mathcal{F}(t,L,L_\|,S_+) \tag{4}$$

and it is independent of the BC. Analogously to Eq. (1), $f_{\mathrm{bulk}}(t)$ can also be decomposed into a singular contribution and a non-singular background:

$$f_{\mathrm{bulk}}(t) = f^{(s)}_{\mathrm{bulk}}(t) + f^{(ns)}_{\mathrm{bulk}}(t) \tag{5}$$

with $f^{(s)}_{\mathrm{bulk}}(t\to 0) \propto |t|^{d\nu} = |t|^{2-\alpha}$, where α is a standard bulk critical exponent. The excess free energy $f^{(\mathrm{s})}_{\mathrm{ex}}$ is defined as the remainder of the free energy density $\mathcal{F}^{(\mathrm{s})}$ after subtraction of the bulk contribution:

$$f^{(\mathrm{s})}_{\mathrm{ex}}(t,L,L_\|,S_+) \equiv \mathcal{F}^{(\mathrm{s})}(t,L,L_\|,S_+) - f^{(\mathrm{s})}_{\mathrm{bulk}}(t). \tag{6}$$

According to Eq. (2) it exhibits the following scaling behavior:

$$f^{(\mathrm{s})}_{\mathrm{ex}}(t,L,L_\|,S_+) = \frac{1}{L^d}\Delta\left(\tau = t\left(L/\xi_0^+\right)^{1/\nu}, \kappa = S_+/L\right). \tag{7}$$

The critical Casimir force F_C per area $L_\|^{(d-1)}$ and per k_BT is defined as

$$F_C \equiv -\frac{\partial\left(L f^{(\mathrm{s})}_{\mathrm{ex}}\right)}{\partial L}\Big|_{t,L_\|,S_+}. \tag{8}$$

Due to Eqs. (2)–(8), the critical Casimir force exhibits the following scaling behavior:

$$F_C\left(t,L,L_\|,S_+\right) = \frac{1}{L^d}\theta\left(\tau = t\left(L/\xi_0^+\right)^{1/\nu}, \kappa = S_+/L\right), \tag{9}$$

where $\theta(\tau,\kappa)$ is a universal scaling function. At the critical point one has $\tau = 0$, so that at criticality the force is given by

$$F_C\left(t=0,L,L_\|,S_+\right) = \frac{1}{L^d}\Theta(\kappa), \tag{10}$$

with

$$\Theta(\kappa) \equiv \theta(0,\kappa). \tag{11}$$

In the limit of very small stripes, i.e., $\kappa \to 0$, the character of a striped surface effectively approaches the one for a homogeneous one with (o) BC. Thus, the scaling functions of the critical Casimir force approach the ones for the critical Casimir force acting on two homogeneous surfaces with $(+,o)$ or (o,o) BC, respectively, i.e.,

$$\theta_{+/o}(\tau,\kappa) \xrightarrow{\kappa\to 0} \begin{cases} \theta_{(+,o)}(\tau), & (+)\ \textit{vs.}\ \text{stripes for } L \gg S_+,\\ \theta_{(o,o)}(\tau), & (o)\ \textit{vs.}\ \text{stripes for } L \gg S_+, \end{cases} \tag{12}$$

where the subscript $+/o$ indicates the corresponding type of BC at the homogeneous surface.

On the other hand for very broad stripes, i.e., $\kappa \to \infty$, the limiting behavior for the case of a homogeneous $(+)$ wall opposite to a striped surface (Fig. 1) is given by the average of the two homogeneous cases for $(+,+)$ and $(+,-)$ BC, respectively. In this case, i.e., for $\kappa \gg 1$ the system effectively corresponds to the one for isolated chemical steps opposite to a homogeneous wall, connecting regions which are almost laterally homogeneous and correspond to $(+,-)$ or $(+,+)$ BC. Thus, for fixed film thickness L, the contributions from the nearly isolated chemical steps to the critical Casimir force per unit area vanish as $\propto P^{-1}$, so that the corresponding contributions to the scaling function vanish as $\propto \kappa^{-1}$. The asymptotic behavior for $L \ll S_+$ of the universal scaling function for the critical Casimir force for a $(+)$ wall *vs.* a striped surface is therefore given by

$$\theta_+(\tau,\kappa\gg 1) - \frac{1}{2}\left(\theta_{(+,+)}(\tau) + \theta_{(+,-)}(\tau)\right) \propto \kappa^{-1}, \tag{13}$$

where the proportionality constant is related to the effects induced by the chemical steps separating the stripes and may depend on τ.

Similarly to Eq. (13), for the case of a (o) wall *vs.* a striped surface (Fig. 2) $\theta(\tau,\kappa)$ approaches

$$\theta_o(\tau,\kappa\gg 1) - \theta_{(+,o)}(\tau) \propto \kappa^{-1}, \tag{14}$$

because $\theta_{(+,o)}(\tau) = \theta_{(-,o)}(\tau)$.

For $\tau < 0$, due to the presence of the chemical steps between the stripes, interfaces form, which separate the domains of positive and negative order parameter. As will be discussed below, for the case of a $(+)$ wall opposite to a striped surface as well as for a (o) wall opposite to a striped surface and $\kappa < 2$, these interfaces align on average *parallel* to the film surfaces. By contrast, for a (o) wall opposite to a striped surface and $\kappa > 2$ the emerging interfaces for $\tau < 0$ preferentially align *perpendicular* to the film surfaces in order to minimize the interface area. As discussed in Sec. VI below, for the latter case the proportionality constant in Eq. (14) is determined by contributions from these interfaces and is given by $-R_\sigma|\tau|^\mu$, where $R_\sigma = \sigma_0(\xi_0^+)^{d-1}/(k_B T_c)$ is the universal amplitude ratio for the interfacial tension $\sigma = \sigma_0|t|^\mu$ associated with the spatially coexisting bulk phases and $\mu = (d-1)\nu$ is its critical exponent. Thus, for the limit $\tau \ll -1$ and $\kappa > 2$ the scaling function of the critical Casimir force between a (o) wall and a striped surface approaches

$$\theta_o(\tau \ll -1, \kappa > 2) \simeq \theta_{(+,o)}(\tau) - \frac{R_\sigma}{\kappa}|\tau|^\mu. \qquad (15)$$

Accordingly, the limits for $\tau \to -\infty$ and $\kappa \to \infty$ do not commute.

III. LATTICE MODEL AND OBSERVABLES

In order to compute the critical Casimir force for a binary liquid mixture close to its critical demixing point, as in Ref. [20] we study the so-called improved Blume-Capel model [48, 49] as a representative of the 3D Ising universality class. It is defined on a three-dimensional simple cubic lattice, with a spin variable S_i on each site i which can take the values $S_i = -1, 0, 1$. The reduced, dimensionless Hamiltonian for nearest neighbor interactions is

$$\mathcal{H} = -\beta \sum_{<ij>} S_i S_j + D \sum_i S_i^2, \qquad S_i = -1, 0, 1, \quad (16)$$

so that the Gibbs weight is $\exp(-\mathcal{H})$ and the partition function is

$$Z(\beta, L, L_\parallel) \equiv \sum_{\{\mathcal{C}\}} \exp(-\mathcal{H}), \qquad (17)$$

where $\{\mathcal{C}\}$ is the configuration space of the Hamiltonian given in Eq. (16). We note that the partition function in Eq. (17) depends implicitly also on the BC (see the discussion below). In line with the convention used in Refs. [20, 29, 45, 50], in the following we shall keep D constant, considering it as a part of the integration measure over $\{S_i\}$, while we vary the coupling parameter β, which is proportional to the inverse temperature, $\beta \sim 1/T$. In the limit $D \to -\infty$, one recovers the usual Ising model, because in this limit any state for which there is an i_0 such that $S_{i_0} = 0$ is suppressed relative to the states $\{S_i = \pm 1\}$. For $d \geq 2$, the model exhibits a phase transition at $\beta_c = \beta_c(D)$ which is second order for $D \leq D_{\mathrm{tri}}$ and first order for $D > D_{\mathrm{tri}}$. The value of D_{tri} in $d = 3$ has been determined as $D_{\mathrm{tri}} = 2.006(8)$ in Ref. [51], as $D_{\mathrm{tri}} \simeq 2.05$ in Ref. [52], and more recently as $D_{\mathrm{tri}} = 2.0313(4)$ in Ref. [53].

We consider a three-dimensional simple cubic lattice $L_z \times L_x \times L_y$, with $L_y = L_x$ and periodic BC in the lateral directions x and y. For the two confining surfaces we employ the BC shown in Figs. 1-4. The BC illustrated in Fig. 1 are realized by fixing the spins at the two surfaces $z = 0$ and $z = L_z - 1$, so that there are $L_z - 2$ layers of fluctuating spins. The spins at the upper surface $z = L_z - 1$ are fixed to $+1$, and the lower surface $z = 0$ mimics a patterned substrate, so that the surface is divided into stripes of equal width s_+ and alternating BC with the spins fixed to $+1$ or -1, respectively.

Here and in the following all lengths are measured in units of the lattice constant a. The size L_z indicates the total number of lattice layers, including eventually the layers of fixed spins. Therefore the thickness L, the lateral size $L_\parallel$, and stripe width S_+ are related to the dimensionless lattice lengths L_z, L_x, and s_+ according to $L = (L_z - 1)a$, $L_\parallel = L_x a$, and $S_+ = s_+ a$, respectively. For the sake of simplicity, here and in the followings Secs. IV-V, we employ a slightly different definition of the scaling variables τ and κ. We consider $\tau_l \equiv t(L_z/\xi_{0l}^+)^{1/\nu}$ and $\kappa_l \equiv s_+/L_z$, where $\xi_{0l}^+ = \xi_0^+/a$ is the dimensionless non-universal amplitude of the correlation length on the *l*attice, measured in units of the lattice constant. Accordingly, we also redefine the aspect ratio as $\rho_l \equiv L_z/L_x$. By comparing these new definitions with the previous ones introduced in Eq. (2), we observe that, for $L \to \infty$, $t(L_z/\xi_{0l}^+)^{1/\nu} = t(L/\xi_0^+)^{1/\nu} + O(1/L)$, $s_+/L_z = S_+/L + O(1/L)$, and $L_z/L_x = L/L_\parallel + O(1/L)$. Therefore, the FSS limit, i.e., the limit $L_z \to \infty$ at fixed τ_l, κ_l, as well as the limit of vanishing aspect ratio $\rho_l \to 0$, are unaltered by these new definitions. In order to avoid a clumsy notation, in the following we omit the index l.

Here we consider the limit of a vanishing aspect ratio $\rho = L_z/L_x \to 0$, which is obtained via extrapolation by computing the critical Casimir force for three different aspect ratios $\rho < 1$ (see the discussion in the following sections). As discussed at the end of Sec. II, for the BC illustrated in Fig. 1, in the limit $\rho \to 0$ the subsequent limit $\kappa \equiv s_+/L_z \to \infty$ corresponds to the presence of an isolated chemical step. In such a geometry, the isolated chemical step gives rise to a line defect which, in turn, results into a linear aspect ratio dependence of the critical Casimir force. In the limit of vanishing aspect ratio the force reduces to the mean value of the force for homogeneous $(+,+)$ and $(+,-)$ BC, for which the two surfaces display the same (resp., opposite) adsorption preference [20] (compare with Eq. (13)). In the opposite limit $\kappa \to 0$, the lower surface is expected to effectively realize Dirichlet BC (compare the upper part of Eq. (12)). In order to analyze this case, as a reference system we study a film geometry $L_z \times L_x \times L_x$ with periodic BC in the lateral directions x and y, fixed spins at the surface $z = L_z - 1$, and open BC on the lower surface, so that there are $L_z - 1$ layers of fluctuating spins. This geometry is illustrated in Fig. 3. In the following, we shall denote this BC as $(+, o)$.

In addition we consider the three-dimensional film geometry $L_z \times L_x \times L_x$ with periodic BC in the lateral directions x and y, with fixed spins at the lower surface $z = 0$, and open BC at the upper surface, so that there are $L_z - 1$ layers of fluctuating spins. For the lower surface $z = 0$ we employ a pattern such that the surface is divided into alternating stripes of equal width s_+ with the spins fixed to either $+1$ or -1. This geometry is illustrated in Fig. 2. Two interesting limiting cases arise from this geometry. In the limit of large stripes, i.e., for $\kappa = s_+/L_z \to \infty$ and for vanishing aspect ratio, the lower surface effectively realizes an isolated chemical step. In analogy with the results of Ref. [20], in this limiting case the critical Casimir force is the mean value of the force for $(+, o)$ and $(-, o)$ BC, which correspond to a film geometry where one of the confining surface implements Dirichlet BC, and the other surface exhibits a homogeneous adsorption preference for one of two components of the fluid. In the absence of an external bulk magnetic field these two BC are equivalent. Therefore we conclude that in the limit $\kappa = s_+/L_z \to \infty$ and for vanishing aspect ratio, the critical Casimir force for the BC of Fig. 2 reduces to the force for the $(+, o)$ BC illustrated in Fig. 3 (compare with Eq. (14)).

In the opposite limit $\kappa \to 0$, the lower surface effectively realizes Dirichlet BC, so that the system reduces to a film geometry with Dirichlet BC on both surfaces (compare with the lower part of Eq. (12)). In order to analyze this limit, as a reference system we consider here a three-dimensional film geometry $L_z \times L_x \times L_x$ with periodic BC in the lateral directions x and y and open BC at both surfaces, so that there are L_z layers of fluctuating spins (see Fig. 4). In the following we shall denote this film BC as (o, o).

For the lattice model corresponding to Eq. (16), the scaling behavior discussed in Eqs. (2), (7), and (9) is valid only up to contributions due to corrections-to-scaling. We distinguish two types of scaling corrections: non-analytic and analytic ones. The non-analytic corrections are due to the presence of irrelevant operators. In this case in Eq. (2) additional scaling field contributions arise, which are characterized by negative RG dimensions. In the FSS limit, i.e., for $L_z \to \infty$, $t \to 0$ at fixed ξ/L_z, this results in the following expression for the singular part of the free energy density $\mathcal{F}^{(s)}$ in the absence of external bulk fields:

$$\mathcal{F}^{(s)}(t, L = a(L_z - 1), L_\parallel = aL_x, S_+ = as_+) = \frac{1}{L_z^d}\left[f(\tau, \kappa, \rho) + \sum_{i,k\geq 1} L_z^{ky_i} g_i(\tau, \kappa, \rho)\right], \quad (18)$$

where $y_i < 0$, $i \geq 1$, are the RG-dimensions of the irrelevant operators and g_i are smooth functions which are universal up to a normalization constant. The leading correction is given by the operator that has the least negative dimension. This is usually denoted by ω, so that the leading scaling corrections are $\propto L_z^{-\omega}$. For the standard three-dimensional Ising model one has $\omega = 0.832(6)$ [45]. In a family of models characterized by an irrelevant parameter λ, it can occur that for a certain choice of λ the amplitude of the leading correction-to-scaling term $\propto L_z^{-\omega}$ vanishes. In these so-called *improved* models, the observed scaling corrections usually decay much more rapidly, i.e., as $L_z^{-\omega_2}$ with $\omega_2 = 1.67(11)$ according to Ref. [54] and $\omega_2 \simeq 1.8867038$ according to Ref. [55] for the three-dimensional Ising universality class. This scenario holds for the Blume-Capel model described by Eq. (16), where D is an irrelevant parameter for $D < D_{\text{tri}}$. At $D = 0.656(20)$ [45] the model is improved. In the present work we fix $D = 0.655$, which is the value of D used in most of the recent simulations of the improved Blume-Capel model [29, 31, 34, 45]. For this value of the reduced coupling D the model is critical for $\beta = \beta_c = 0.387721735(25)$ [45].

Another type of scaling corrections is provided by so-called analytic scaling corrections, which can stem from various sources. Nonlinear terms in the expansion of the scaling field τ [56] result in scaling corrections $\propto L_z^{-1/\nu}$. Analytic corrections can also be due to the boundary conditions: BC which are not periodic in all directions induce additional corrections, which are proportional to L_z^{-1}. It was first proposed in Ref. [57] in the context of studying surface susceptibilities, that such scaling corrections can be absorbed by the substitution $L_z \to L_z + c$, where c is a non-universal, temperature–independent length. Recently, this property has been checked numerically in Refs. [26, 58, 59] for the XY model with free surfaces, in Ref. [29] for the Ising model with homogeneously fixed surface spins, and in Refs. [20, 31] for the Ising model with laterally inhomogeneous surfaces.

Here we study the critical Casimir force using the improved Blume-Capel model according to Eq. (16). On the basis of the above discussion, for such a model the leading scaling corrections are expected to be proportional to L_z^{-1}. Furthermore, assuming that also in this case in leading order such a scaling correction can be absorbed by the substitution $L_z \to L_z + c$, Eq. (9) is replaced by

$$F_C\left(t, L = a(L_z - 1), L_\parallel = aL_x, S_+ = as_+\right) = \frac{1}{(L_z + c)^3}\theta\left(t\left(\frac{L_z + c}{\xi_{0l}^+}\right)^{1/\nu}, \frac{s_+}{L_z + c}\right). \quad (19)$$

In the case of laterally homogeneous BC in Figs. 3 and 4, the dimensionless quantity c (such that ca is a length) enters only via the volume factor and via the scaling variable τ. Scaling corrections to Eq. (19) are expected to decay as $\propto L_z^{-\omega_2}$ (with $\omega_2 = 1.67(11)$ [54] or $\omega_2 \simeq 1.8867038$ [55], see above).

We introduce the reduced energy density $E(\beta, L_z, L_x, s_+)$ in units of $-k_BT$, which is used in order to compute the critical Casimir force:

$$E(\beta, L_z, L_x, s_+) \equiv \frac{1}{V}\left\langle \sum_{<ij>} S_i S_j \right\rangle, \tag{20}$$

where $V \equiv L_z L_x^2$ is the total number of spins and $\langle \dots \rangle$ denotes the thermal average. (Note that, according to Eq. (16), $-\frac{\partial \mathcal{H}}{\partial \beta}$ has no contribution $\sim \sum_i S_i^2$.) The reduced free energy density $F(\beta, L_z, L_x, s_+)$ is defined as

$$\begin{aligned} &F(\beta, L_z, L_x, s_+) \\ &\quad \equiv \frac{1}{V} \ln\left(\frac{Z(\beta, L = a(L_z-1), L_\parallel = aL_x)}{Z(0, L = a(L_z-1), L_\parallel = aL_x)}\right). \end{aligned} \tag{21}$$

Thus $F(\beta, L_z, L_x, s_+)$ is the free energy per spin and in units of $-k_B T$. It is normalized such that $F(\beta = 0, L_z, L_x, s_+) = 0$. With this normalization one has

$$F(\beta, L_z, L_x, s_+) = \int_0^\beta d\beta' E(\beta', L_z, L_x, s_+). \tag{22}$$

The relation between $\mathcal{F}(t, L_z, L_x, s_+)$ and the reduced free energy density $F(\beta, L_z, L_x, s_+)$ defined in Eq. (21) is given by

$$\begin{aligned} &F(\beta, L_z, L_x, s_+) \\ &\quad = -\mathcal{F}(t, L = a(L_z-1), L_\parallel = aL_x, S_+ = as_+) \\ &\quad + \mathcal{F}(t \to \infty, L = a(L_z-1), L_\parallel = aL_x, S_+ = as_+). \end{aligned} \tag{23}$$

Finally, the reduced bulk free energy density $F_{\mathrm{bulk}}(\beta)$ is defined by taking the thermodynamic limit of Eq. (21):

$$F_{\mathrm{bulk}}(\beta) = \lim_{L_z, L_x \to \infty} F(\beta, L_z, L_x, s_+). \tag{24}$$

IV. CRITICAL CASIMIR AMPLITUDE AT T_c

In order to determine the critical Casimir force at T_c, we follow the approach introduced in Ref. [24] and also used in Refs. [20, 25, 32], which we briefly describe here. For two reduced Hamiltonians $\mathcal{H}_1$ and $\mathcal{H}_2$ associated with the same configuration space $\{C\}$ we construct the convex combination $\mathcal{H}(\lambda)$

$$\mathcal{H}(\lambda) \equiv (1-\lambda)\,\mathcal{H}_1 + \lambda \mathcal{H}_2, \qquad \lambda \in [0,1]\,. \tag{25}$$

This Hamiltonian $\mathcal{H}(\lambda)$ leads to a free energy $\mathrm{F}(\lambda)$ in units of $k_B T$ [60]. Its derivative is

$$\frac{\partial \mathrm{F}(\lambda)}{\partial \lambda} = \frac{\sum_{\{C\}} \frac{\partial \mathcal{H}(\lambda)}{\partial \lambda} e^{-\mathcal{H}(\lambda)}}{\sum_{\{C\}} e^{-\mathcal{H}(\lambda)}}. \tag{26}$$

Combining Eqs. (25) and (26) we can determine the free energy difference as

$$\mathrm{F}(1) - \mathrm{F}(0) = \int_0^1 d\lambda \frac{\partial \mathrm{F}(\lambda)}{\partial \lambda} = \int_0^1 d\lambda \langle \mathcal{H}_2 - \mathcal{H}_1 \rangle_\lambda, \tag{27}$$

where $\langle \mathcal{H}_2 - \mathcal{H}_1 \rangle_\lambda$ is the thermal average of the observable $\mathcal{H}_2 - \mathcal{H}_1$ with the statistical weight $\exp(-\mathcal{H}(\lambda))$. For every λ this average is accessible to standard MC simulations. Finally the integral appearing in Eq. (27) is performed numerically, yielding the free energy difference between the systems governed by the Hamiltonians $\mathcal{H}_2$ and $\mathcal{H}_1$, respectively.

We apply Eq. (27) with $\mathcal{H}_1$ as the Hamiltonian of the lattice $L_z \times L_x \times L_x$ with the BC illustrated in Figs. 1-4, and $\mathcal{H}_2$ as the Hamiltonian of the lattice $(L_z - 1) \times L_x \times L_x$ plus a completely separated two-dimensional layer of non-interacting spins governed by the reduced Hamiltonian of Eq. (16) with $\beta = 0$, so that both Hamiltonians share the same configuration space. This layer can be inserted into the film by varying the coupling $(1-\lambda)\beta$ with its neighboring planes between 0 and β. With this we evaluate the following quantity:

$$I\,(\beta, L_z, L_x, s_+) \equiv \frac{1}{L_x^2} \int_0^1 d\lambda \langle \mathcal{H}_2 - \mathcal{H}_1 \rangle_\lambda. \tag{28}$$

By using the definitions of the excess free energy (Eq. (6)) and of the critical Casimir force (Eq. (8)) one finds [20]

$$\begin{aligned} &I\,(\beta, L_z, L_x, s_+) = F_{\mathrm{bulk}}(\beta) \\ &\quad + F_C\left(t, L = a\left(L_z - \frac{3}{2}\right), L_\parallel = aL_x, S_+ = as_+\right), \end{aligned} \tag{29}$$

where corrections $\propto L_z^{-2}$ have been neglected. In computing the critical Casimir force, the derivative in Eq. (8) is implemented by a finite difference between the free energies of a film of thickness $L = a(L_z - 1)$ and of a film of thickness $L - a = a(L_z - 2)$, so that the resulting critical Casimir force corresponds to the intermediate thickness $a(L_z - 3/2)$. This choice ensures that in the FSS limit no additional scaling corrections $\propto L_z^{-1}$ are generated [20]. By inserting Eq. (19) into Eq. (29) we obtain the following scaling form for $I\,(\beta, L_z, L_x, s_+)$:

$$\begin{aligned} &I\,(\beta, L_z, L_x, s_+) = F_{\mathrm{bulk}}(\beta) \\ &\quad + \frac{1}{\left(L_z - \frac{1}{2} + c\right)^3} \theta\left(t\left(\frac{L_z - \frac{1}{2} + c}{\xi_0^+}\right)^{1/\nu}, \frac{s_+}{L_z - \frac{1}{2} + c}\right). \end{aligned} \tag{30}$$

At the bulk critical temperature Eq. (30) turns into

$$\begin{aligned} &I\,(\beta_c, L_z, L_x, s_+) = F_{\mathrm{bulk}}(\beta_c) \\ &\quad + \frac{1}{(L_z - 1/2 + c)^3} \Theta\left(\frac{s_+}{L_z - 1/2 + c}\right). \end{aligned} \tag{31}$$

Equation (31) can be rewritten as

$$\begin{aligned} &I\,(\beta_c, L_z, L_x, s_+) = F_{\mathrm{bulk}}(\beta_c) \\ &\quad + \frac{1}{(L_z - 1/2 + c\,')^3} \Theta\left(\kappa = \frac{s_+}{L_z}\right) + O\left(L_z^{-3}\left(\frac{c}{L_z}\right)^2\right), \end{aligned} \tag{32}$$

with $c\,'$ given by

$$c\,' = c + \left(c - \frac{1}{2}\right) \frac{\kappa}{3\Theta(\kappa)} \frac{\partial\Theta(\kappa)}{\partial\kappa}. \quad (33)$$

In a series of MC simulations, we have evaluated the quantity $I\,(\beta_c, L_z, L_x, s_+)$ for lattice sizes $L_z = 8$, 12, 16, 24, 32, and 48 with the BC illustrated in Fig. 1 for $\kappa = 1/4$, 1/2, 1, 2, and 3 as well as with the BC of Fig. 3, which corresponds to the limit $\kappa \to 0$. We have also computed $I\,(\beta_c, L_z, L_x, s_+)$ for lattice sizes $L = 8$, 12, 16, 24, and 32 with the BC illustrated in Fig. 2 for $\kappa = 1/4$, 1/2, 3/4, 1, 2, and 3 as well as with BC of Fig. 4, which corresponds to the limit $\kappa \to 0$. Certain important details of the simulations are reported in App. A. Since we are interested in the film geometry, which corresponds to the limit of a vanishing aspect ratio $\rho = L_z/L_x$, we have simulated every BC for three aspect ratios $\rho \leq 1/8$, such that there is always an even number of stripes in the lower confining surface. An odd or non-integer number of stripes would give rise to a line defect which in turn, for $\rho \to 0$, would result into an unwelcome linear aspect-ratio dependence [20]. Within the present numerical accuracy, for $\rho \leq 1/8$ the MC data do not show a visible dependence on ρ. Thus we consider our results obtained for non-vanishing $\rho \leq 1/8$ as a reliable extrapolation to the limit $\rho \to 0$. A posteriori, this also justifies the scaling ansatz in Eqs. (7)-(11), in which the dependence on ρ has been neglected. We have simulated the Blume-Capel model with the Hamiltonian given in Eq. (16), choosing the values of the reduced couplings as $D = 0.655$ and $\beta_c = 0.387721735$. This corresponds to the critical point of the improved model [45], for which the Eq. (32) is expected to describe correctly the corrections to scaling. We have fitted our MC data directly to the quantity $I\,(\beta_c = 0.387721735, L_z, L_x, s_+)$ in Eq. (32), leaving $F_{\mathrm{bulk}}(\beta_c)$, Θ, and $c\,'$ as free parameters. In order to control a possible systematic error due to subleading scaling corrections, we have repeated the fits discarding the smallest lattices. For the BC of Figs. 1 and 3, and for various values of ratio κ, in Tables I and II we report the fit results as a function of the smallest lattice size L_{min} taken into account for the fit. In Tables III and IV we report the corresponding fit results for the BC of Figs. 2 and 4.

Inspection of the the fit results tells that we generally reach a good χ^2/DOF ratio and the results appear to be stable with respect to the choice of L_{min}. (DOF is the number of degrees of freedom, i.e., the number of statistically independent points minus the number of fit parameters) While there is a clear dependence of the Casimir amplitude Θ on κ, as expected the critical bulk free energy density $F_{\mathrm{bulk}}(\beta_c)$ does not exhibit a dependence on κ. Furthermore the latter is in agreement with the value $F_{\mathrm{bulk}}(\beta_c) = 0.0757368(4)$ reported in Ref. [29]. By conservatively judging the variation of the resulting Θ with respect to L_{min}, from Tables I and II we obtain the following estimates for the BC shown in Figs. 1 and 3:

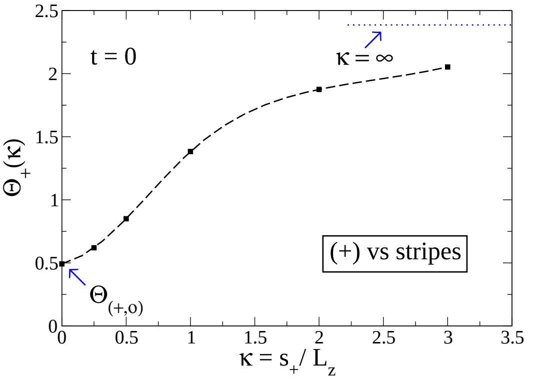

FIG. 5. Critical Casimir force amplitude $\Theta_+(\kappa) = \theta_+(0,\kappa)$ (see Eqs. (9) and (11)) at T_c for the BC of Figs. 1 and 3 and for $\kappa = S_+/L = 0$, 1/4, 1/2, 1, 2, and 3 as inferred from Tables I and II (see Eqs. (34)-(39)). The amplitude at $\kappa = 0$ is obtained for the $(+, o)$ BC illustrated in Fig. 3. The dashed line provides a smooth interpolation. This line saturates at $\Theta_+(\kappa \to \infty) = \left(\Theta_{(+,+)} + \Theta_{(+,-)}\right)/2 = 2.386(5)$ [20], which is indicated by the dotted line. The omitted statistical error bars defined as one standard deviation and calculated with the standard Jackknife method (see, e.g., Ref. [62]) are comparable with the symbol size.

$$(+) \text{ vs stripes:} \quad \Theta_+(\kappa = 0) = \Theta_{(+,o)} = 0.492(5), \quad (34)$$

$$\Theta_+(\kappa = 1/4) = 0.62(1), \quad (35)$$

$$\Theta_+(\kappa = 1/2) = 0.85(1), \quad (36)$$

$$\Theta_+(\kappa = 1) = 1.383(4), \quad (37)$$

$$\Theta_+(\kappa = 2) = 1.875(6), \quad (38)$$

$$\Theta_+(\kappa = 3) = 2.053(5). \quad (39)$$

The subscript + indicates the homogeneous (+) BC on one of the confining surfaces. These amplitudes are shown in Fig. 5. As expected, for decreasing values of κ the critical Casimir amplitude $\Theta(\kappa)$ approaches the corresponding value for $(+, o)$ BC. In particular, $\Theta_+(\kappa = 1/4)$ is only 26% larger than $\Theta_+(0)$. In the opposite limit $\kappa \to \infty$, $\Theta_+(\kappa)$ approaches the critical Casimir amplitude for a single chemical step: $\Theta_+(\kappa \to \infty) = 2.386(5)$ [20]. In particular, $\Theta_+(\kappa = 3)$ is only 14% smaller than $\Theta_+(\kappa \to \infty)$. In the whole sampled region, $\Theta_+(\kappa)$ is a positive and monotonically increasing function of κ so that the critical Casimir force at T_c is always repulsive. The critical Casimir amplitude $\Theta_+(0) = \Theta_{(+,o)}$ for $(+, o)$ BC can be compared with, e.g., the amplitude $\Theta_{(+,+)}$ resulting from homogeneous BC $(+, +)$, for which the two confining surfaces exhibit the same adsorption preference. Within mean-field theory one has $\Theta_{(+,o)}/\Theta_{(+,+)} = -1/4$ [21]. According to the MC results of Ref. [29], one has $\Theta_{(+,+)} = -0.820(15)$ so that the ratio between the two amplitudes is $\Theta_{(+,o)}/\Theta_{(+,+)} = -0.60(1)$. Thus the fluctuations produce a significant dependence of this ratio on the spatial dimension. Accordingly, one concludes that in $d = 3$ mean-field theory captures only the qualitative behavior of the critical Casimir force. Our result

$L_{\min}$	$\kappa \to 0 : (+, o)$	$\kappa = 1/4$	$\kappa = 1/2$
8	$\chi^2/DOF = 8.7/15$	$\chi^2/DOF = 12.3/15$	$\chi^2/DOF = 16.1/15$
	$F_{\rm bulk}(\beta_c) = 0.0757369(2)$	$F_{\rm bulk}(\beta_c) = 0.0757369(1)$	$F_{\rm bulk}(\beta_c) = 0.0757375(1)$
	$\Theta_+ = 0.492(5)$	$\Theta_+ = 0.622(5)$	$\Theta_+ = 0.845(5)$
	$c\,' = 0.36(3)$	$c\,' = -0.48(2)$	$c\,' = -0.44(1)$
12	$\chi^2/DOF = 8.0/12$	$\chi^2/DOF = 7.5/12$	$\chi^2/DOF = 13.2/12$
	$F_{\rm bulk}(\beta_c) = 0.0757368(2)$	$F_{\rm bulk}(\beta_c) = 0.0757368(2)$	$F_{\rm bulk}(\beta_c) = 0.0757375(2)$
	$\Theta_+ = 0.495(10)$	$\Theta_+ = 0.634(11)$	$\Theta_+ = 0.84(1)$
	$c\,' = 0.40(9)$	$c\,' = -0.39(7)$	$c\,' = -0.44(5)$
16	$\chi^2/DOF = 7.4/9$	$\chi^2/DOF = 6.5/9$	$\chi^2/DOF = 7.7/9$
	$F_{\rm bulk}(\beta_c) = 0.0757368(2)$	$F_{\rm bulk}(\beta_c) = 0.0757368(2)$	$F_{\rm bulk}(\beta_c) = 0.0757372(2)$
	$\Theta_+ = 0.50(2)$	$\Theta_+ = 0.63(2)$	$\Theta_+ = 0.88(2)$
	$c\,' = 0.4(2)$	$c\,' = -0.39(15)$	$c\,' = -0.23(12)$

TABLE I. Fit of our MC data at T_c for the BC of Figs. 3 and 1, to Eq. (32) with free parameters $F_{\rm bulk}(\beta_c)$, $\Theta_+(\kappa = s_+/L_z)$, and $c\,'$. $L_{\min}$ is the smallest lattice size taken into account for the fit. DOF denotes degrees of freedom. The quoted error bars of the fit parameters correspond to one standard deviation; see, e.g., Ref. [61] for a discussion of the method of minimum χ^2 data fitting.

$L_{\min}$	$\kappa = 1$	$\kappa = 2$	$\kappa = 3$
8	$\chi^2/DOF = 8.9/15$	$\chi^2/DOF = 12.7/15$	$\chi^2/DOF = 9.0/15$
	$F_{\rm bulk}(\beta_c) = 0.0757370(1)$	$F_{\rm bulk}(\beta_c) = 0.0757366(1)$	$F_{\rm bulk}(\beta_c) = 0.0757369(1)$
	$\Theta_+ = 1.383(4)$	$\Theta_+ = 1.875(5)$	$\Theta_+ = 2.053(4)$
	$c\,' = -0.264(8)$	$c\,' = -0.138(8)$	$c\,' = -0.097(5)$
12	$\chi^2/DOF = 4.8/12$	$\chi^2/DOF = 11.0/12$	$\chi^2/DOF = 7.0/12$
	$F_{\rm bulk}(\beta_c) = 0.0757369(2)$	$F_{\rm bulk}(\beta_c) = 0.0757367(2)$	$F_{\rm bulk}(\beta_c) = 0.0757369(2)$
	$\Theta_+ = 1.387(8)$	$\Theta_+ = 1.869(8)$	$\Theta_+ = 2.048(8)$
	$c\,' = -0.25(2)$	$c\,' = -0.15(2)$	$c\,' = -0.11(2)$
16	$\chi^2/DOF = 4.2/9$	$\chi^2/DOF = 7.1/9$	$\chi^2/DOF = 5.0/9$
	$F_{\rm bulk}(\beta_c) = 0.0757369(2)$	$F_{\rm bulk}(\beta_c) = 0.0757368(2)$	$F_{\rm bulk}(\beta_c) = 0.0757369(2)$
	$\Theta_+ = 1.394(12)$	$\Theta_+ = 1.86(1)$	$\Theta_+ = 2.05(1)$
	$c\,' = -0.22(5)$	$c\,' = -0.18(4)$	$c\,' = -0.09(3)$

TABLE II. Same as Table I for $\kappa = s_+/L_z = 1$, 2, 3 and for the BC of Fig. 1.

$L_{\min}$	$\kappa \to 0 : \ (o, o)$	$\kappa = 1/4$	$\kappa = 1/2$
8	$\chi^2/DOF = 6.9/12$	$\chi^2/DOF = 7.5/12$	$\chi^2/DOF = 13.7/12$
	$F_{\rm bulk}(\beta_c) = 0.07573678(9)$	$F_{\rm bulk}(\beta_c) = 0.0757369(1)$	$F_{\rm bulk}(\beta_c) = 0.0757369(1)$
	$\Theta_o = -0.030(2)$	$\Theta_o = -0.039(2)$	$\Theta_o = -0.054(1)$
	$c\,' = 0.8(2)$	$c\,' = 0.02(9)$	$c\,' = 0.07(6)$
12	$\chi^2/DOF = 3.7/9$	$\chi^2/DOF = 3.8/9$	$\chi^2/DOF = 11.0/9$
	$F_{\rm bulk}(\beta_c) = 0.0757368(1)$	$F_{\rm bulk}(\beta_c) = 0.0757370(2)$	$F_{\rm bulk}(\beta_c) = 0.0757369(2)$
	$\Theta_o = -0.030(5)$	$\Theta_o = -0.045(5)$	$\Theta_o = -0.053(3)$
	$c\,' = 0.7(7)$	$c\,' = 0.5(4)$	$c\,' = 0.0(3)$
16	$\chi^2/DOF = 3.2/6$	$\chi^2/DOF = 2.5/6$	$\chi^2/DOF = 7.5/6$
	$F_{\rm bulk}(\beta_c) = 0.0757368(3)$	$F_{\rm bulk}(\beta_c) = 0.0757369(3)$	$F_{\rm bulk}(\beta_c) = 0.0757368(3)$
	$\Theta_o = -0.035(15)$	$\Theta_o = -0.038(10)$	$\Theta_o = -0.05(1)$
	$c\,' = 1.5 \pm 2.3$	$c\,' = -0.2 \pm 1.2$	$c\,' = -0.1(9)$

TABLE III. Same as Table I for the BC of Figs. 4 and 2.

$L_{\rm min}$	$\kappa = 3/4$	$\kappa = 1$	$\kappa = 2$	$\kappa = 3$
8	$\chi^2/DOF = 9.9/12$	$\chi^2/DOF = 8.0/12$	$\chi^2/DOF = 13.1/12$	$\chi^2/DOF = 12.0/12$
	$F_{\rm bulk}(\beta_c) = 0.07573679(9)$	$F_{\rm bulk}(\beta_c) = 0.0757370(1)$	$F_{\rm bulk}(\beta_c) = 0.0757365(2)$	$F_{\rm bulk}(\beta_c) = 0.0757368(2)$
	$\Theta_o = -0.062(2)$	$\Theta_o = -0.032(2)$	$\Theta_o = 0.185(4)$	$\Theta_o = 0.287(4)$
	$c\,' = 0.37(6)$	$c\,' = 1.3(2)$	$c\,' = 0.34(5)$	$c\,' = 0.36(4)$
12	$\chi^2/DOF = 7.4/9$	$\chi^2/DOF = 7.9/9$	$\chi^2/DOF = 8.9/9$	$\chi^2/DOF = 8.3/9$
	$F_{\rm bulk}(\beta_c) = 0.0757367(1)$	$F_{\rm bulk}(\beta_c) = 0.0757370(2)$	$F_{\rm bulk}(\beta_c) = 0.0757369(3)$	$F_{\rm bulk}(\beta_c) = 0.0757366(3)$
	$\Theta_o = -0.058(4)$	$\Theta_o = -0.032(5)$	$\Theta_o = 0.173(9)$	$\Theta_o = 0.292(10)$
	$c\,' = 0.1(2)$	$c\,' = 1.2(7)$	$c\,' = 0.04(20)$	$c\,' = 0.45(14)$
16	$\chi^2/DOF = 4.4/6$	$\chi^2/DOF = 3.4/6$	$\chi^2/DOF = 5.6/6$	$\chi^2/DOF = 6.6/6$
	$F_{\rm bulk}(\beta_c) = 0.0757369(3)$	$F_{\rm bulk}(\beta_c) = 0.0757367(2)$	$F_{\rm bulk}(\beta_c) = 0.0757361(6)$	$F_{\rm bulk}(\beta_c) = 0.0757363(6)$
	$\Theta_o = -0.07(1)$	$\Theta_o = -0.021(8)$	$\Theta_o = 0.20(3)$	$\Theta_o = 0.30(2)$
	$c\,' = 0.9(8)$	$c\,' = -0.8 \pm 1.7$	$c\,' = 0.9(6)$	$c\,' = 0.65(35)$

TABLE IV. Same as Table III for $\kappa = s_+/L_z = 3/4$, 1, 2, 3 and for the BC of Fig. 2

for $\Theta_+(\kappa = 0) = \Theta_{(+,o)} = 0.492(5)$ is in agreement with the result $\Theta_{(+,o)} = 0.497(3)$ of Ref. [31], while it is not compatible with the earlier results [21] $\Theta_{(+,o)} = 0.33$ and 0.416 obtained with the $\varepsilon-$expansion method and 0.375(14) obtained by MC simulations [21].

Inspecting the results reported in Tables III and IV, we obtain the following estimates for the BC shown in Figs. 2 and 4:

$$(o) \text{ vs stripes:} \quad \Theta_o(\kappa = 0) = \Theta_{(o,o)} = -0.030(5) \quad (40)$$

$$\Theta_o(\kappa = 1/4) = -0.039(6), \quad (41)$$

$$\Theta_o(\kappa = 1/2) = -0.053(3), \quad (42)$$

$$\Theta_o(\kappa = 3/4) = -0.062(4), \quad (43)$$

$$\Theta_o(\kappa = 1) = -0.032(3), \quad (44)$$

$$\Theta_o(\kappa = 2) = 0.18(1), \quad (45)$$

$$\Theta_o(\kappa = 3) = 0.287(5), \quad (46)$$

where the subscript o indicates the homogeneous Dirichlet BC on one of the two confining surfaces. These amplitudes are shown in Fig. 6. As expected, for decreasing values of κ the critical Casimir amplitude $\Theta_o(\kappa)$ approaches the corresponding value $\Theta_{(o,o)}$ for (o,o) BC, while in the opposite limit $\kappa \to \infty$ it approaches slowly the value $\Theta_{(+,o)}$ for $(+,o)$ BC. Moreover, the critical Casimir amplitude changes sign: it is attractive for $\kappa = 0$ and repulsive for $\kappa \to \infty$. Inspecting Fig. 6, we can estimate that $\Theta_o(\kappa)$ vanishes for $\kappa \approx 1.2$. Remarkably, different than $\Theta_+(\kappa)$ in Fig. 5, the critical Casimir amplitude $\Theta_o(\kappa)$ is not monotonic, but exhibits a minimum close at $\kappa \approx 3/4$. Our result for $\Theta_o(\kappa = 0) = \Theta_{(o,o)} = -0.030(5)$ is in agreement with the recent MC result $\Theta_o(\kappa = 0) = \Theta_{(o,o)} = -0.028(16)$ of Ref. [32] and also with the earlier results [21] $\Theta_o(0) = -0.0278$ and -0.0328 obtained with the $\varepsilon-$expansion method and $\Theta_o(0) = -0.023(4)$ obtained by MC simulations [21].

Finally, we can test the validity of Eq. (33) by studying the behavior of the scaling corrections in the limit $\kappa \to 0$. To this end, we consider the BC of Fig. 1 and we take the limit of $\kappa \to 0$ at fixed L_z, i.e., $s_+ \to 0$ in Eq. (31).

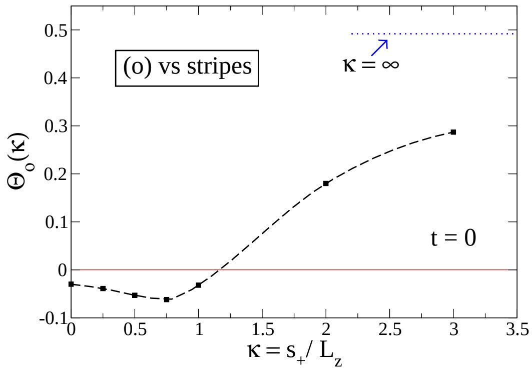

FIG. 6. Critical Casimir force amplitude $\Theta_o(\kappa) = \theta_o(0,\kappa)$ (see Eqs. (9) and (11)) at T_c for the BC of Figs. 2 and 4 and for $\kappa = S_+/L = 0$, 1/4, 1/2, 3/4, 1, 2, 3, as inferred from Tables III and IV (Eqs. (40)-(46)). The amplitude at $\kappa = 0$ is obtained for the (o,o) BC illustrated in Fig. 4. The dashed line provides a smooth interpolation. This line saturates at $\Theta(\kappa \to \infty) = \Theta_{(+,o)} = 0.492(5)$ (Eq. (34)), which is indicated by the dotted line. The comparison with the thin full line tells that $\Theta_o(\kappa)$ changes sign at $\kappa \approx 1.2$. The omitted statistical error bars are comparable with the symbol size.

Assuming that $\Theta(\kappa)$ is analytic close to $\kappa = 0$, we obtain

$$I\left(\beta_c, L_z, L_x, s_+ \to 0\right) = F_{\rm bulk}(\beta_c) + \frac{\Theta_+(0)}{(L_z - 1/2 + c)^3}. \quad (47)$$

A comparison of Eq. (47) with Eq. (32) gives $c\,'(\kappa \to 0) = c$, a result which could also be obtained by taking the limit $\kappa \to 0$ in Eq. (33). On the other hand, in the limit $s_+ \to 0$, the system effectively realizes the BC shown in Fig. 3, but still in the presence of only $L_z - 2$ fluctuating layers of spins (as for the BC in Fig. 1 with $s_+ > 0$). According to the convention fixed in Sec. III, this corresponds to $(+,o)$ BC for a film with $L_z - 1$ layers and thickness $a(L_z-2)$:

$$\begin{aligned} I\left(\beta_c, L_z, L_x, s_+\to 0\right) &= I_{(+,o)}\left(\beta_c, L_z-1, L_x\right) \\ &= F_{\text{bulk}}(\beta_c) + \frac{\Theta_{(+,o)}}{(L_z-1-1/2+c'_{(+,o)})^3}, \end{aligned} \tag{48}$$

where the subscript $(+,o)$ denotes explicitly the BC of Fig. 3 with the convention of Sec III and where we have used Eq. (32). By comparing Eq. (47) with Eq. (48) we finally obtain:

$$\lim_{\kappa\to 0} c\,'(\kappa) = c = c\,'_{(+,o)} - 1. \tag{49}$$

We can extract $c\,'_{(+,o)} = 0.36(4)$ from the fit results of Table I for the $(+,o)$ BC. This result is in marginal agreement with the result $c\,'_{(+,o)} = 0.42(2)$ of Ref. [31] in which the same improved Blume-Capel Hamiltonian as the present one has been simulated [63]. Using Eq. (49) we obtain $c = c\,'(\kappa\to 0) = -0.64(4)$. Inspecting the fit results of Tables I and II, we observe that $c\,'(\kappa)$ varies smoothly with κ and indeed approaches the value of $c = -0.64(4)$ for $\kappa\to 0$. According to the results of Eqs. (34)-(39) and due to Fig. 5, the coefficient multiplying $(c-1/2)$ in Eq. (33) is positive. This would imply that, due to $c-1/2<0$, $c\,'(\kappa)<c$. However, within the current numerical precision such an inequality appears to be not satisfied by the fit results reported in Tables I and II. This suggests that the ansatz of Eq. (19) does not completely capture the scaling corrections for the striped BC. One may need to modify in addition the second scaling argument of θ in Eq. (19), for example by replacing L with $L+aN$, with N an integer number depending on the convention used to measure the film thickness, or more generally, by introducing a second non-universal length. A similar analysis of the scaling corrections for the BC shown in Fig. 2 is beyond the presently available numerical precision.

V. THE CRITICAL CASIMIR FORCE SCALING FUNCTION

The determination of the critical Casimir force off criticality has been performed using essentially the algorithm introduced in Ref. [23] and also used in Refs. [26–29, 31]. By using the definition of the critical Casimir force given in Eq. (8), the definition of the reduced free energy density given in Eq. (21), and the definition of the reduced bulk free energy density given in Eq. (24), the critical Casimir force can be expressed as

$$\begin{aligned} F_C\left(t, L=a\left(L_z-\frac{3}{2}\right), L_\parallel = aL_x, S_+ = as_+\right) \\ = \Delta F(\beta, L_z, L_x, s_+) - F_{\text{bulk}}(\beta), \end{aligned} \tag{50}$$

where

$$\begin{aligned} \Delta F(\beta, L_z, L_x, s_+) \equiv{} & L_z F(\beta, L_z, L_x, s_+) \\ & - (L_z-1)F(\beta, L_z-1, L_x, s_+). \end{aligned} \tag{51}$$

Analogous to Eq. (29), in Eq. (50) the derivative in Eq. (8) is implemented by a finite difference between the free energies of a film of thickness $L=a(L_z-1)$ and of a film of thickness $L-a=a(L_z-2)$, so that the resulting critical Casimir force corresponds to the intermediate thickness $a(L_z-3/2)$. This choice ensures that in the FSS limit no additional scaling corrections $\propto L_z^{-1}$ are generated [20]. The reduced temperature t is given by $t=(\beta_c-\beta)/\beta$, with $\beta_c = 0.387721735(25)$ [45]. As in Eq. (29), in Eq. (50) corrections $\propto L_z^{-2}$ have been neglected. We note that $\Delta F(\beta, L_z, L_x, s_+)\to F_{\text{bulk}}(\beta)$ for $L_z, L_x\to\infty$, which is in accordance with the vanishing of the critical Casimir force in the limit of large volume. Another useful relation follows from a comparison of Eqs. (50) and (29):

$$\Delta F(\beta, L_z, L_x, s_+) = I\left(\beta, L_z, L_x, s_+\right). \tag{52}$$

Instead of using the coupling parameter approach as in Sec. IV, here we compute the free energy differences by sampling the internal energy density $E(\beta, L_z, L_x, s_+)$ for various values of β and for film thicknesses $a(L_z-1)$ and $a(L_z-2)$. Then $\Delta F(\beta, L_z, L_x, s_+)$ is computed by a numerical integration of Eq. (22). For doing so, it is very useful to observe that it is not necessary to perform the integral in full between $\beta'=0$ and $\beta'=\beta$ [29]. In fact, by inserting a lower cut-off β_0 into the integral appearing in Eq. (22) one can effectively compute the difference between the critical Casimir force and the force at the inverse temperature β_0. This implies that the critical Casimir force can be expressed as

$$\begin{aligned} & F_C\left(t, L=a\left(L_z-\frac{3}{2}\right), L_\parallel = aL_x, S_+ = as_+\right) \\ &= \Delta\widehat{F}(L_z, L_x, s_+; \beta, \beta_0) - (F_{\text{bulk}}(\beta) - F_{\text{bulk}}(\beta_0)) \\ &+ F_C\left(t_0, L=a\left(L_z-\frac{3}{2}\right), L_\parallel = aL_x, S_+ = as_+\right), \end{aligned} \tag{53}$$

with

$$\begin{aligned} \Delta\widehat{F}(L_z, L_x, s_+; \beta, \beta_0) \equiv{} & L_z\int_{\beta_0}^{\beta} d\beta' E(\beta', L_z, L_x, s_+) \\ & -(L_z-1)\int_{\beta_0}^{\beta} d\beta' E(\beta', L_z-1, L_x, s_+), \end{aligned} \tag{54}$$

and $t_0 = (\beta_c-\beta_0)/\beta_0$ as the reduced temperature corresponding to the lower cutoff β_0. Since for $L=a(L_z-1)\gg\xi$ the critical Casimir force vanishes $\propto\exp(-L/\xi)$, one can neglect the last term in Eq. (53) if the correlation length ξ at the lower cutoff β_0 is much smaller than $L=a(L_z-1)$. Moreover, due to Eqs. (52) and (50) the last term in Eq. (53) can be calculated independently with the coupling parameter approach described in Sec. IV. This provides a precise control of any approximation involving the cutoff β_0. We did compute $F_C\left(t_0, L=a\left(L_z-\frac{3}{2}\right), L_\parallel = aL_x, S_+ = as_+\right)$ within the aforementioned coupling parameter approach and we have taken into account this term in Eq. (53) whenever it is relevant within the statistical precision. The numerical integrations in Eq. (54) have been carried out according to Simpson's rule. Certain technical details are reported in App. A. Finally, the determination of the critical Casimir force on the basis of Eq. (53) requires the knowledge of the reduced bulk free energy density $F_{\text{bulk}}(\beta)$ which is independent of the BC. We have determined it via MC simulations of lattices size L_z^3 with $L_z = 24 - 256$ and periodic BC. In App. B we report certain details of this computation, which is important for a successful determination of F_C.

Along these lines we have computed the critical Casimir force for lattice thickness $L_z = 8$, 12, 16, and 24 with the BC shown in Figs. 1 and 3 as well as for $\kappa = 0$, 1/2, 1, 2, and 3. As in Sec. IV we have considered three aspect ratios for each value of L_z and κ: we have taken $\rho = 1/8$, 1/12, and 1/16 for $\kappa \leq 2$, as well as $\rho = 1/12$, 1/18, and 1/24 for $\kappa = 3$. We have checked that for these small values the data are independent of ρ within the statistical accuracy. Therefore we expect that our results capture the limit $\rho \to 0$

In the present case, for $t \neq 0$ it is not easy to subtract the scaling corrections because according to Eq. (19) a part of the scaling corrections $\propto 1/L_z$ stem from the dependence on L_z of the second scaling argument of θ. This holds even if the scaling ansatz of Eq. (19) does not completely capture the $1/L_z$ scaling corrections: in fact, the non-universal length $c\,'$, defined in Eq. (33) and extracted from the fits reported in Tables I and II, shows a small but significant dependence on κ, which would be absent if scaling corrections were independent of κ. In Ref. [20] a similar problem was encountered in the MC investigation of the critical Casimir force in the presence of an isolated chemical step. There the dependence of the force on the aspect ratio contributes to the scaling corrections. Since this dependence on ρ was found to be linear, in that case it was possible to eliminate the scaling corrections via a first-order Taylor expansion of the critical Casimir force in ρ. As Figs. 5 and 6 show, in the present case the critical Casimir force does not follow such a simple dependence on κ. Furthermore, the possible values of κ which can be sampled by the MC simulations are constrained by the fact that the stripe width s_+ has to be an integer number. Due to these technical difficulties, here we implement an approximate scheme for the removal of the scaling corrections. For every value of κ we extract the non-universal length $c\,'$ from the fits of Tables I and II. Then we employ the substitution $L_z \to L_z + c\,'$. Since such a substitution cannot completely eliminate the scaling corrections $\propto L_z^{-1}$, the resulting scaling function $\theta(\tau, \kappa)$ exhibits a residual scaling correction $\propto \psi(\tau, \kappa)/L_z$, where $\psi(\tau, \kappa)$ is a scaling function. By construction, we have $\psi(0, \kappa) = 0$. Thus, since ψ is a continuous function, there is an interval around $\tau = 0$ in which the residual scaling corrections are negligible with respect to the numerical precision. Furthermore, for $\kappa \to 0$ and $\kappa \to \infty$ this method becomes exact and thus we have $\psi(\tau, \kappa \to 0) = \psi(\tau, \kappa \to \infty) = 0$. Therefore, the interval of validity around $\tau = 0$ is expected to increase as κ is lowered towards 0 or is increased toward ∞.

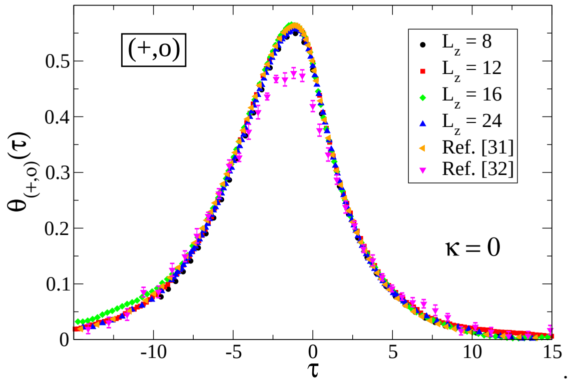

FIG. 7. The universal scaling function $\theta_{(+,o)}(\tau)$ of the critical Casimir force for the BC $(+,o)$ shown in Fig. 3, corresponding to the limit $\kappa = s_+/L_z \to 0$ of the BC shown in Fig. 1. Scaling corrections have been subtracted by using $c\,' = 0.36(4)$ (see the main text). We also compare our results with those of Ref. [31] for $L = 16$ and of Ref. [32] for $L = 20$. The omitted statistical error bars are, apart from $\tau \lesssim -10$, comparable with the symbol size.

In Fig. 7 we show our results for the BC shown in Fig. 3, corresponding to the limit $\kappa = s_+/L_z \to 0$ of the BC shown in Fig. 1. In order to normalize the scaling variable τ, one needs the value of the non-universal amplitude ξ_{0l}^+ of the correlation length ξ. From Ref. [29] we infer $\xi_{0l}^+ = 0.4145(4)$ in units of the lattice constant. As for the critical exponent ν, we use the recent MC result $\nu = 0.63002(10)$ of Ref. [45]. In Fig. 7 we also compare our results with those of Refs. [31] and [32]. We observe a perfect agreement with the results of Ref. [31], which in fact have been obtained by simulating precisely the same improved Blume-Capel model. The comparison with the results of Ref. [32] is less satisfactory and reveals a difference between the curves around the position of their maximum in the low-temperature phase, i.e., $\tau < 0$. This difference may be due to the fact that the Ising model simulated in Ref. [32] suffers from larger scaling corrections than the improved model used here, which makes the extrapolation of the FSS limit more difficult. For the BC illustrated in Fig. 1, in Figs. 8, 9, 10, 11, and 12 we show our results for the scaling function $\theta_+(\tau, \kappa)$, for $\kappa = 1/4$, 1/2, 1, 2, and 3, respectively.

Inspection of Figs. 7-12 reveals a satisfactory scaling collapse for the lattice sizes considered here. This supports the validity of the procedure described above to eliminate the scaling corrections. In Fig. 13 we show a comparison of the critical Casimir force for $\kappa = 0$, 1/4, 1/2, 1, 2, and 3, as obtained for $L_z = 24$. We also com-

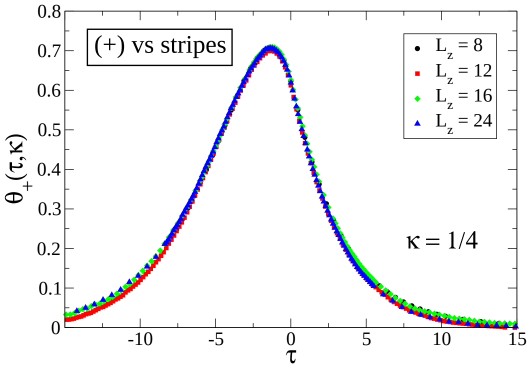

FIG. 8. The universal scaling function $\theta_+(\tau, \kappa)$ of the critical Casimir force for the BC shown in Fig. 1 with $\kappa = S_+/L = 1/4$ and $c\,' = -0.48(2)$. The omitted statistical error bars are comparable with the symbol size.

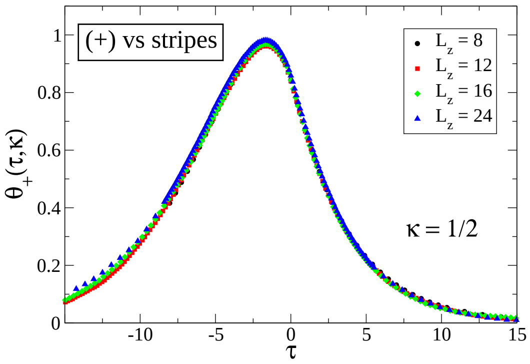

FIG. 9. Same as Fig. 8 for $\kappa = 1/2$ and $c\,' = -0.44(1)$.

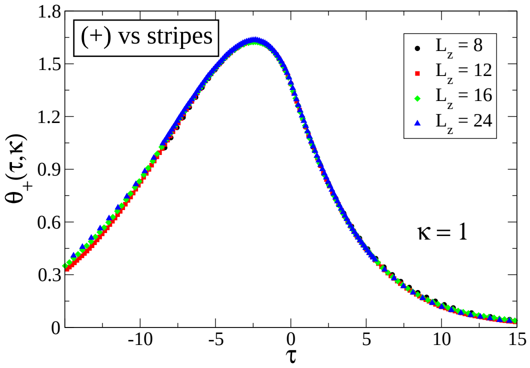

FIG. 10. Same as Fig. 8 for $\kappa = 1$ and $c\,' = -0.26(1)$.

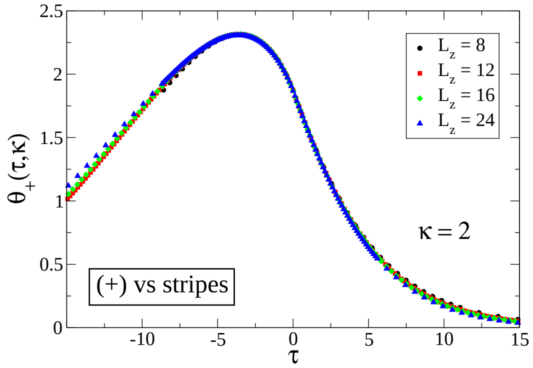

FIG. 11. Same as Fig. 8 for $\kappa = 2$ and $c\,' = -0.14(1)$.

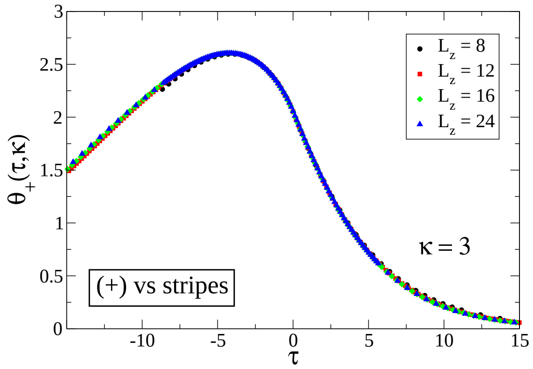

FIG. 12. Same as Fig. 8 for $\kappa = 3$ and $c\,' = -0.10(1)$.

pare the present results with the universal scaling function which describes the critical Casimir force for an isolated chemical step in the limit of vanishing aspect ratio, as determined in Ref. [20]. This system corresponds to the limit $\kappa \to \infty$ and results in the mean value of the critical Casimir force for laterally homogeneous $(+,+)$ and $(+,-)$ BC. In the whole range $0 \leq \kappa \leq \infty$ the critical Casimir force is always repulsive. This is expected because the stripe width for $(+)$ and for $(-)$ BC are equal and the repulsive critical Casimir force for $(+,-)$ BC is stronger than the attractive one for $(+,+)$ BC [25]. In Fig. 13 we also show a comparison with the mean value of the critical Casimir force for the homogeneous $(+,+)$ and $(+,-)$ BC, as obtained by MC simulations in Refs. [25, 29].

In Fig. 14 we show our results for the (o,o) BC shown in Fig. 4, corresponding to the limit $\kappa = s_+/L_z \to 0$ of the BC (o) vs stripes shown in Fig. 2. We also compare our results with those of Ref. [25] for the approximants (i) and (ii) presented therein. The approximant (i) agrees with our results for $\tau \gtrsim -6$, whereas the approximant

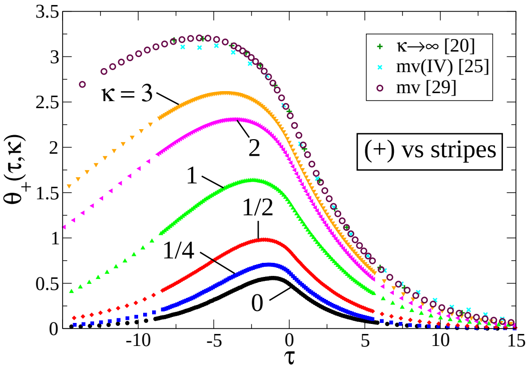

FIG. 13. Comparison of the universal scaling function $\theta_+(\tau,\kappa)$ for $\kappa = 0$, $1/4$, $1/2$, 1, 2, and 3 as determined with $L = 24$. We compare the data also with the scaling function $\theta_+(\tau,\kappa \to \infty)$ in the limit of vanishing aspect ratio ρ, as obtained in Ref. [20] with $L = 16$. The limit $\kappa \to \infty$ corresponds to the critical Casimir force between a homogeneous $(+)$ surface and a surface with an isolated chemical step which, for $\rho \to 0$, results in the *m*ean *v*alue of the critical Casimir force for laterally homogeneous $(+,+)$ and $(+,-)$ BC [20]. We compare the results also with those latter mean values, which are either extracted from the so-called approximant IV of Ref. [25] (mv (IV)) or which stem from the results of Ref. [29] (mv).

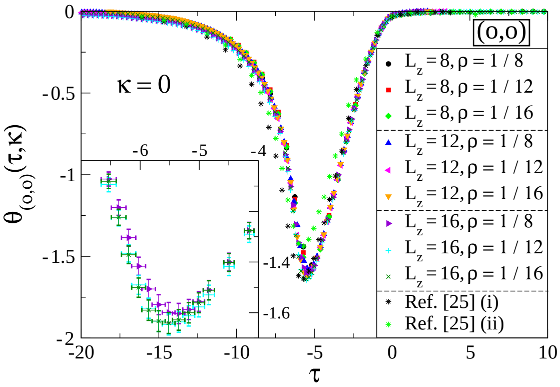

FIG. 14. Universal scaling function $\theta_{(o,o)}(\tau)$ of the critical Casimir force for the BC (o,o) shown in Fig. 4, corresponding to the limit $\kappa = s_+/L_z \to 0$ of the BC shown in Fig. 2. Scaling corrections have been subtracted by using $c\,' = 0.8(2)$ (see the main text). We compare our results with those of Ref. [25] obtained from the approximants (i) and (ii) presented therein and for the film thickness $L = 20$. The inset provides a magnification of the resulting curves close to the minimum of the force, for the largest available film thickness $L = 16$ and for the three aspect ratios $\rho \equiv L_z/L_x$ considered here.

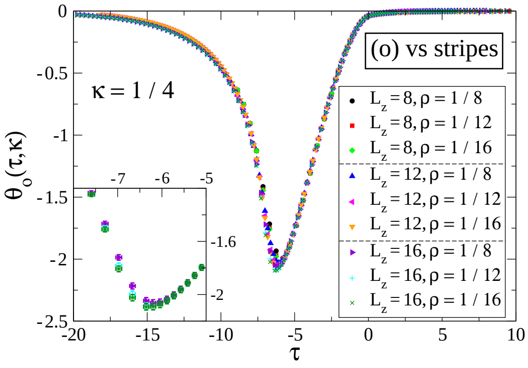

FIG. 15. Universal scaling function $\theta_o(\tau,\kappa)$ of the critical Casimir force for the BC shown in Fig. 2 with $\kappa = s_+/L_z = 1/4$ and $c\,' = 0.02(9)$. The data points for $L = 8$ and $\rho = 1/8$, $1/12$ are hardly visible because they overlap with the other data sets. The inset provides a magnification of the resulting curves close to the minimum of the force, for the largest available film thickness $L = 16$ and for the three aspect ratios $\rho \equiv L_z/L_x$ considered here.

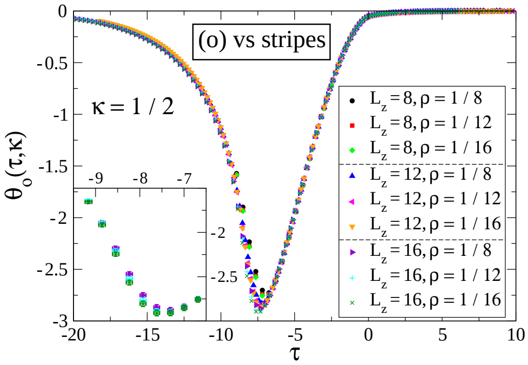

FIG. 16. Same as Fig. 15 for $\kappa = 1/2$ and $c\,' = 0.05(8)$.

(ii) displays a systematic deviation from our results. For $\tau \lesssim -6$ both approximants show a disagreement with our results. While the approximant (ii) displays a small but visible deviation from our results, the approximant (i) exhibits a larger, systematic deviation from our results. Such deviations may be due to the difficulty in extrapolating the FSS limit of the Ising model used in Ref. [25], which exhibits larger scaling corrections than the improved model of Eq. (16). For the BC illustrated in Fig. 2, in Figs. 15, 16, 17, 18, and 19 we show our results for the scaling function $\theta_o(\tau,\kappa)$, for $\kappa = 1/4$, $1/2$, $3/4$, 1, and 3, respectively.

The numerical determination of the critical Casimir forces in the presence of a Dirichlet BC at one of the two confining surfaces has turned out to be much more in-

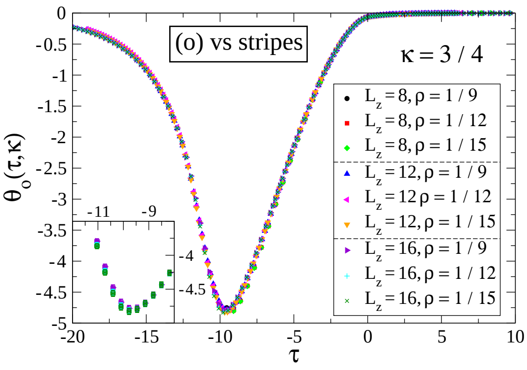

FIG. 17. Same as Fig. 15 for $\kappa = 3/4$ and $c\,' = 0.37(7)$.

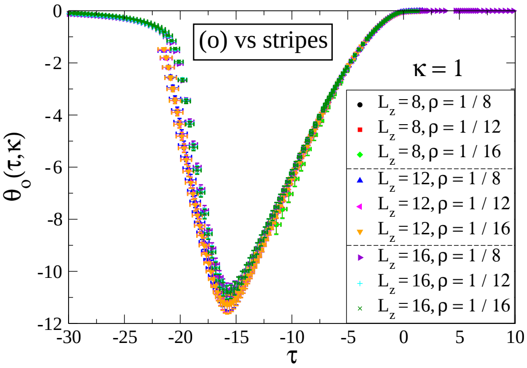

FIG. 18. Same as Fig. 15 for $\kappa = 1$ and $c\,' = 1.3(2)$.

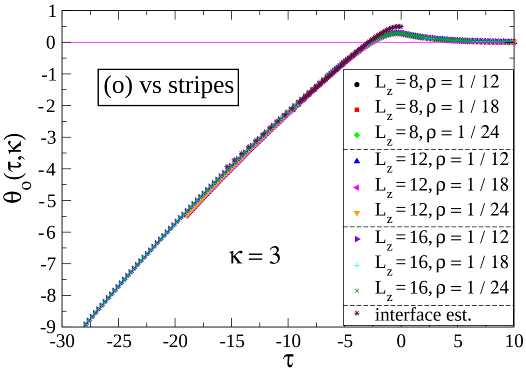

FIG. 19. Same as Fig. 15 for $\kappa = 3$ and $c\,' = 0.36(9)$. We also compare our results with the interface estimate given by the r.h.s. of Eq. (15). The scaling function changes sign at $\tau = \tau_0 \simeq -2.7$.

volved than the computation for the BC of Figs. 1 and 3. First, at variance with the previous cases, we observed the onset of a dependence of the critical Casimir force on the aspect ratio $\rho = L_z/L_x$. As illustrated in the insets of Figs. 14-19, such a dependence on ρ appears in a narrow interval of τ in the low-temperature phase. Although small, the differences between the calculated scaling functions $\theta_o(\tau, \kappa)$ for the three aspect ratios considered here is visible and larger than the statistical error bars [64]. The observed dependence on ρ implies the onset of a lateral correlation length, associated with an ordering process in the low temperature phase. In order to understand this point, it is useful to consider the limit $\beta \to \infty$, i.e., the ground state of the model with the BC illustrated in Figs. 2 and 4. For the BC shown in Fig. 4, it is easy to see that the ground state is a spatially homogeneous state in which all spins take the same value. For the BC shown in 2, besides the homogeneous state, one can consider also a “striped” state, in which each spin in the film takes the value corresponding to the underlying stripe, so that the configuration of the system consists of columns of cross sectional area $s_+ \times L_x$ and height L_z. In view of the periodic BC in the two lateral directions, the area $\mathcal{A}$ of the interface between + and − spins is given by

$$\begin{aligned} \mathcal{A} &= \frac{L_x^2}{2}, && \text{homogeneous state,} \\ \mathcal{A} &= \frac{L_x}{s_+} L_z L_x = \frac{L_x^2}{\kappa}, && \text{striped state.} \end{aligned} \tag{55}$$

Thus, at low temperature, the system orders in a homogeneous state for $\kappa < 2$ and in a striped state for $\kappa > 2$. As a function of the parameter κ, the ground state undergoes a first-order transition at $\kappa = 2$. Moreover, for $\kappa = 2$, besides the homogeneous and the striped ground states, there are other states which have the same (minimal) energy: such states can be obtained by flipping the value of the spins in a single column in the striped state. We note that the number of these additional ground states diverges in the thermodynamic limit. The emergence of these ground states at $\kappa = 2$ gives rise to a sort of glassy behavior at low temperatures, which results in a considerable technical difficulty in simulating these systems. We leave this issue for future research.

This lateral ordering process at low temperatures corresponds to a phase transition which occurs in the film geometry characterized by the BC described by Figs. 2 and 4. This causes the dependence on the aspect ratio exhibited in Figs. 14-19. We note that, for the BC corresponding to Figs. 1 and 3, the striped state is never a ground state. Moreover, without an external bulk field the presence of a surface field at the upper surface rounds the transition between the paramagnetic high-temperature phase and the homogeneous ground state to a simple crossover. This is in agreement with the independence of ρ observed in Figs. 7-12. The appearance of a lateral correlation length breaks the scaling behavior discussed in Sec. II. On the other hand, inspection of Figs. 14-19 reveals that the data for the two smallest aspect ratios agree within the statistical error. Therefore, since one expects a smooth dependence of the scaling function $\theta_o(\tau,\kappa)$ on ρ, in particular in the limit of $\rho \to 0$, we can regard our results for the smallest aspect ratio as a reliable extrapolation of the limit $\rho \to 0$.

Another difficulty in the numerical determination of the critical Casimir force for the BC shown in Figs. 2 and 4 lies in the fact that the scaling function $\theta_o(\tau,\kappa)$ exhibits a minimum in the low-temperature phase which is shifted towards more negative values of τ upon increasing κ. Thus, in order to study this important feature of the scaling function, one has to generate MC data for temperatures lower than the ones needed for the BC shown in Figs. 1 and 3. Upon lowering the temperature the simulations become increasingly difficult because of the appearance of many metastable states associated with the aforementioned ground-state phase transition at $\kappa = 2$.

Finally, in order to eliminate the leading scaling corrections, we have implemented the procedure outlined above. We note that for the BC shown in Fig. 2 such a method appears to be less reliable. While for $\kappa \leq 1/2$ and $\kappa = 3$ the overall scaling collapse is good, for $\kappa = 3/4$ and for sufficiently negative values of τ, there is a small but systematic deviation between the data for lattice size $L = 12$ and $L = 16$. The scaling collapse is even worse for $\kappa = 1$; in this case a further complication seems to be that, apparently, in this case scaling corrections are stronger (see Table IV).

According to the discussion in Sec. III, for the BC shown in Fig. 2 in the limit $\kappa \to \infty$ one expects to recover the BC shown in Fig. 3. Since for $\kappa = 0$ the force is always attractive (see Fig. 14) and for $\kappa \to \infty$ the force is repulsive (see Fig. 7), at a certain intermediate value of κ the force has to change sign. According to Fig. 6, at criticality this occurs at $\kappa = \kappa_0 \approx 1.2$. Besides a change of sign of the force as a function of κ there is also a change of sign as a function of τ. This is nicely illustrated in Fig. 19, where for $\kappa = 3$ the force is found to be repulsive (resp. attractive) for $\tau \geq \tau_0$ (resp. $\tau \leq \tau_0$), with $\tau_0 \approx -2.7$. This implies that in the scaling regime and for a given temperature $T < T_c$, i.e., $t = (T - T_c)/T_c < 0$ the force is repulsive (resp. attractive) for $L < L_0(t)$ (resp. $L > L_0(t)$), with $L_0(t) = \xi_{0l}(\tau_0/t)^{\nu}$. Therefore $L = L_0(t)$ is a mechanically stable point of equilibrium for the critical Casimir force which can be sensitively tuned by varying the reduced temperature. This can be exploited for levitation purposes [41]. In Fig. 19 we also compare our result with the interface estimate, i.e., the r.h.s. of Eq. (15), which is expected to hold for $\kappa > 2$ and $\tau \ll -1$. To this end, we employ the estimate of the universal amplitude ratio $R_\sigma = 0.377(11)$ [65]. The interface estimate is in nice agreement with our MC results for $\tau \lesssim -3.5$.

In Fig. 20 we show a comparison of the scaling function $\theta_o(\tau,\kappa)$ of the critical Casimir force for the BC shown in Fig. 2 for $\kappa = 0$, 1/4, 1/2, 3/4, 1, and 3 as determined with $L = 16$ and with the smallest aspect ratio ρ available. We also compare these results with the Casimir scaling functions for the BC $(+,o)$ shown in Fig. 3, which corresponds to the limit $\kappa \to \infty$. Figure 20 suggests that the approach of the limit $\kappa \to \infty$ is somehow singular. Apparently, for every finite value of κ, the force becomes attractive for sufficiently negative values of τ and exhibits a minimum which deepens and shifts to more negative values of τ as κ is increased. Simultaneously, the zero of $\theta_o(\tau,\kappa)$ shifts towards lower values of τ.

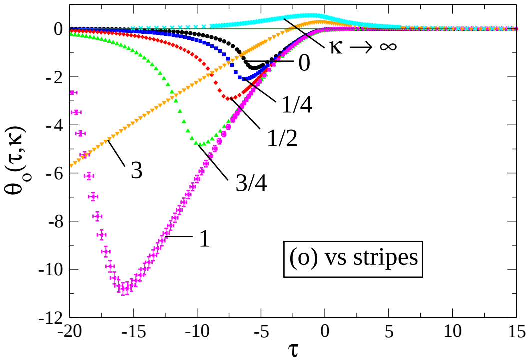

FIG. 20. Comparison of the universal scaling function $\theta_o(\tau,\kappa)$ for $\kappa = 0$, 1/4, 1/2, 3/4, 1, and 3 for the BC (o) vs stripes shown in Fig. 2, as determined with $L = 16$ and the smallest aspect ratio ρ available. We compare these data also with the scaling function $\theta_o(\tau,\kappa \to \infty) = \theta_{(+,o)}(\tau)$, as obtained in Fig. 7 with $L = 24$. For further discussions see the main text.

VI. MEAN-FIELD THEORY

Within the field-theoretic approach, bulk and surface critical phenomena of the Ising universality class are described by the standard Landau-Ginzburg-Wilson fixed-point Hamiltonian given by [4, 5, 66]

$$\mathcal{H}[\phi] = \int_V \mathrm{d}^d r \left\{ \frac{1}{2}(\nabla\phi)^2 + \frac{\tilde{\tau}}{2}\phi^2 + \frac{u}{4!}\phi^4 \right\} + \int_{\partial V} \mathrm{d}^{(d-1)} r \left\{ \frac{c(\mathbf{r})}{2}\phi^2 - h_1(\mathbf{r})\phi \right\}, \quad (56)$$

where $\phi(\mathbf{r})$ is the spatially varying order parameter describing the critical medium, which completely fills the volume V bounded by the boundaries ∂V in d-dimensional space. In Eq. (56) $\tilde{\tau} \propto t$ and $u > 0$ is a coupling constant providing stability for $t < 0$; $c(\mathbf{r})$ is the surface enhancement, which, within mean-field theory, can be interpreted as an inverse extrapolation length of the order parameter field, and $h_1(\mathbf{r})$ is an (external) surface field acting on the order parameter at the boundaries. Here, we consider surface fields and enhancements which can be different for the two confining surfaces and which may also vary along one lateral direction of a single surface. In the strong adsorption limit, i.e., $(\pm)$ BC, corresponding to the so-called normal surface UC, the surface behavior is described by the renormalization-group fixed-point values $h_1 \to \pm\infty$, and the order parameter diverges close to the surface: $\phi|_{\partial V} \to \pm\infty$. The ordinary surface UC corresponds to the fixed point values $\{c = \infty, h_1 = 0\}$ and a vanishing order parameter $\phi|_{\partial V} = 0$, i.e., Dirichlet (o) BC. The film geometry considered here is bounded by surfaces at $z = 0$ and at $z = L$ with either homogeneous $(+)$ or (o) BC or periodically alternating $(+)/(-)$ BC of width $S_+ = P/2$ along the lateral x-direction (see Figs. 1–4).

The Hamiltonian given in Eq. (56) is minimized by the mean-field order parameter profile $m \equiv u^{1/2}\langle\phi\rangle$: $\delta\mathcal{H}[\phi]/\delta\phi|_{\phi=u^{-1/2}m} = 0$. Renormalization group arguments tell that mean-field theory (MFT) provides the correct universal properties of critical phenomena for spatial dimensions above the upper critical dimension $d \geq d_{\mathrm{uc}} = 4$ (up to logarithmic corrections in $d = d_{\mathrm{uc}}$). Mean-field theory provides the lowest order contribution to universal properties within an expansion in terms of $4 - d = \varepsilon$. Thus, universal properties in $d = 4$ can be determined from MFT, up to two independent non-universal amplitudes appearing in the description of bulk critical phenomena (two-scale universality [4, 5]): the amplitude B of the bulk order parameter $\langle\phi\rangle = \pm B|t|^{\beta}$ for $t < 0$, where $\beta(d = 4) = 1/2$, and the amplitude ξ_0^+ of the correlation length [see Eq. (3), where $\nu(d = 4) = 1/2$]. Since here we are dealing only with vanishing or diverging values of h_1 and c, within MFT all quantities appearing in Eq. (56) can be expressed in terms of these amplitudes: $\tilde{\tau} = t(\xi_0^+)^{-2}$ and $u = 6(B\xi_0^+)^{-2}$. Using the stress tensor method [21] the mean-field universal scaling functions of the critical Casimir forces at the upper critical dimension $d_{\mathrm{uc}} = 4$ can be inferred directly from the MFT order parameter profiles up to an overall prefactor $\propto u^{-1}$.

For the laterally homogeneous $(+,+)$, $(+,-)$, $(+,o)$, or (o,o) BC the MFT order parameter profiles across the film [21, 67] and the corresponding universal scaling functions of the critical Casimir force are known analytically [21, 68]. Accordingly, the critical Casimir amplitude $\Theta_{(+,+)} = 8K^4(1/\sqrt{2})(B\xi_0^+)^2 \simeq -47.2682(B\xi_0^+)^2$, where $K(k)$ is the complete elliptic integral of the first kind [21]. Note that, within MFT, the scaling functions $\theta_{(+,-)}(\tau) = -4\theta_{(+,+)}(-\tau/2)$ [69], and $\theta_{(+,o)}(\tau) = \theta_{(+,-)}(4\tau)/16$ [21] are directly related to each other, so that at T_c $\Theta_{(+,-)} = -4\Theta_{(+,+)}$ and $\Theta_{(+,o)} = -\Theta_{(+,+)}/4$. In contrast to the case $d = 3$, the MFT scaling function for (o,o) BC vanishes for $\tau \geq 0$ (i.e., $\Theta_{(o,o)}(d = 4) = 0$) and exhibits a cusp-like singularity at its minimum at $\tau = -\pi^2$ below which $\theta_{(o,o)}(\tau < -\pi^2) = \theta_{(+,+)}(\tau)$ and above which an analytic expression for $\theta_{(o,o)}$ has been derived in Ref. [68].

In order to obtain the spatially inhomogeneous MFT order parameter profile for the film geometry involving chemically striped surfaces, we have minimized $\mathcal{H}[\phi]$ numerically using a quadratic finite element method. Here, we extend previous investigations [38] to negative values $t < 0$ and to a broader range of geometrical parameters. The corresponding scaling functions for the critical Casimir force are obtained via the stress tensor [21].

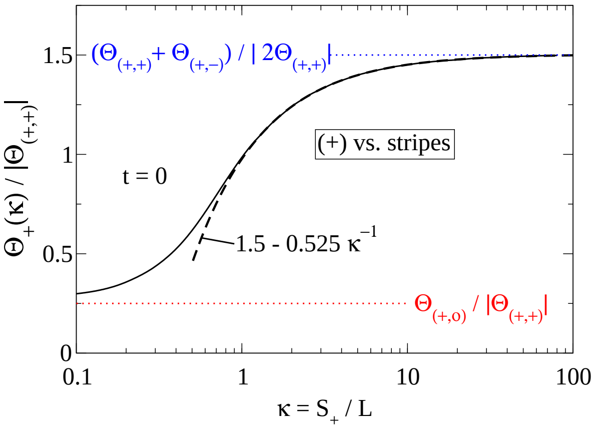

FIG. 21. Reduced critical Casimir force amplitude $\Theta_+(\kappa)$ [Eq. (11)] in units of $|\Theta_{(+,+)}|$ for the BC shown in Fig. 1 as obtained within mean-field theory. For $\kappa \to 0$ the Casimir amplitude approaches the value for $(+,o)$ BC shown in Fig. 3, i.e., $\Theta_{(+,o)}/|\Theta_{(+,+)}| = \frac{1}{4}$, indicated by the lower red dotted line. For large stripes, $\Theta_+(\kappa \to \infty)/|\Theta_{(+,+)}|$ approaches the average value of the reduced Casimir amplitudes for $(+,+)$ and $(+,-)$ BC, i.e., $(\Theta_{(+,+)} + \Theta_{(+,-)})/|2\Theta_{(+,+)}| = \frac{3}{2}$ shown as upper blue dotted line. For $\kappa \gg 1$ the behavior of the Casimir amplitude $\Theta_+(\kappa)/|\Theta_{(+,+)}|$ approaches the function $\frac{3}{2} - \frac{5}{4}\alpha_+\kappa^{-1}$ (see the black dashed line and the main text). From a least square fit we have obtained $\alpha_+ = 0.420(4)$. Compare Fig. 5, where $\Theta_{(+,o)}/|\Theta_{(+,+)}| = 0.60(1)$ and $\Theta_+(\kappa \to \infty)/|\Theta_{(+,+)}| \simeq 2.91(5)$.

The boundary condition for the diverging order parameter profile at those parts of the surface where there are $(+)$ or $(-)$ BC can be implemented numerically only approximately via a short-distance expansion of the corresponding profile for the semi-infinite systems [4, 5]. Thus, the MFT data presented below are subject to a numerical error which contains also the uncertainties due to the fineness of the numerical mesh. We estimate the numerical error for the data presented below to be less than 1% or $\pm 0.004 \times |\Theta_{(+,+)}|$ if the latter is bigger.

A. Critical Casimir amplitude at T_c

In Fig. 21 the amplitude of the critical Casimir force $\Theta_+(\kappa) = \theta_+(0, \kappa)$ (see Eqs. (9) and (11)) for a striped surface opposite to a homogeneous surface with $(+)$ BC is shown as obtained numerically within MFT in units of $|\Theta_{(+,+)}|$. We have been able to calculate the values of $\Theta_+(\kappa)$ numerically within the range $\kappa = 0.1$ to $\kappa = 80$. As discussed above, for $\kappa \to 0$ the Casimir amplitude approaches the value for $(+,o)$ BC shown in Fig. 3, i.e., $\Theta_{(+,o)}$, so that for relatively narrow stripes the chemically striped wall effectively mimics a wall with (o) BC. On the other hand, for $\kappa \to \infty$ the Casimir amplitude approaches the average value of the Casimir

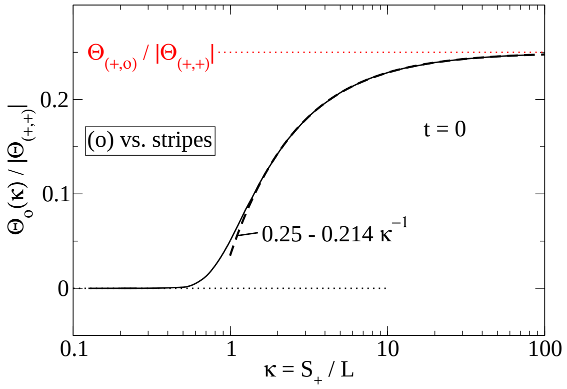

FIG. 22. Reduced Casimir amplitude $\Theta_o(\kappa)$ [Eq. (11)] in units of $|\Theta_{(+,+)}|$ for the BC shown in Fig. 2 as obtained within MFT. For $\kappa \to 0$ the Casimir amplitude approaches monotonically from positive values the limiting value $\Theta_{(o,o)} = 0$ shown by the lower green dotted line. According to Eq. (14), for $\kappa \gg 1$ the reduced Casimir amplitude $\Theta_o(\kappa)/|\Theta_{(+,+)}|$ approaches $\frac{1}{4}(1 - \alpha_o\kappa^{-1})$ shown as black dashed line. From a least square fit we have obtained, within MFT, $\alpha_o = 0.857(9)$ [Eq. (58)]. For $\kappa \to \infty$, $\Theta_o(\kappa)/|\Theta_{(+,+)}|$ approaches the Casimir amplitude for $(+,o)$ BC, i.e., $\Theta_{(+,o)}/|\Theta_{(+,+)}| = 1/4$ shown as the upper red dotted line. Compare Fig. 6, where $\Theta_o(\kappa = 0)/|\Theta_{(+,+)}| = 0.037(6)$ and $\Theta_o(\kappa \to \infty)/|\Theta_{(+,+)}| = 0.60(1)$.

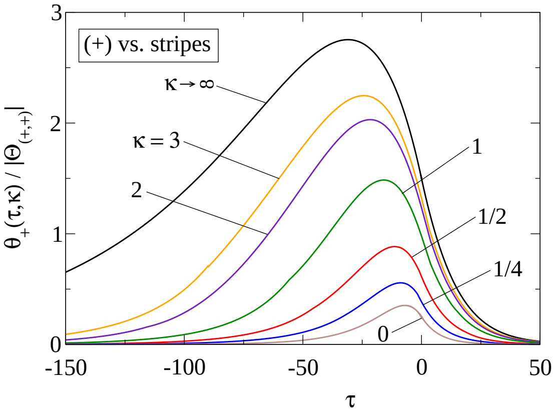

FIG. 23. Reduced universal scaling function $\theta_+(\tau,\kappa)/|\Theta_{(+,+)}|$ [Eq. (9)] for a striped surface opposite to a surface with homogeneous (+) BC (Fig. 1), as determined numerically within MFT for various values of κ. For $\kappa \to 0$ and $\kappa \to \infty$, the reduced scaling functions approach their limiting behaviors $\theta_{(+,o)}(\tau)/|\Theta_{(+,+)}|$ [Eq. (12)] and $(\theta_{(+,+)}(\tau) + \theta_{(+,-)}(\tau))/|2\Theta_{(+,+)}|$ [Eq. (13)], respectively. Compare Fig. 13 by taking into account that there, i.e., in $d = 3$, $|\Theta_{(+,+)}| = 0.820(15)$.

amplitudes for $(+,+)$ and $(+,-)$ BC, i.e., $\Theta_+(\kappa \to \infty) = (\Theta_{(+,+)} + \Theta_{(+,-)})/2 = -\frac{3}{2}\Theta_{(+,+)}$, whereas $\Theta_+(\kappa)$ monotonically interpolates between these two limits.

For $\kappa \gg 1$, according to Eq. (13), we find for the critical Casimir amplitude

$$\begin{aligned}&\Theta_+(\kappa \gg 1)\\ &\simeq \Theta_{(+,o)} + \left(\frac{\Theta_{(+,+)} + \Theta_{(+,-)}}{2} - \Theta_{(+,o)}\right)\left(1 - \frac{\alpha_+}{\kappa}\right)\\ &\qquad = -\,\Theta_{(+,+)}\left(\frac{3}{2} - \frac{5}{4}\alpha_+\kappa^{-1}\right), \qquad (57)\end{aligned}$$

where the proportionality constant α_+ has been determined within MFT as $\alpha_+ = 0.420(4)$ by using a least-square fit.

Figure 22 shows the reduced critical Casimir force amplitude $\Theta_o(\kappa)$ in units of $|\Theta_{(+,+)}|$ for the case of a striped surface opposite to a surface with a homogeneous (o) BC (see Figs. 2 and 4). Similar to Fig. 21, $\Theta_o(\kappa)$ monotonically interpolates between the limiting values for $\kappa \to 0$ and $\kappa \to \infty$, i.e., $\Theta_{(o,o)}/|\Theta_{(+,+)}| = 0$ and $\Theta_{(+,o)}/|\Theta_{(+,+)}| = 1/4$, respectively. For small stripes the amplitude $\Theta_o(\kappa \to 0)$ approaches its limit already for larger values of κ than in the case of a homogeneous (+) BC shown in Fig. 21. This indicates that the strength of the tendency of a chemically striped surface to effectively mimic an (o) BC in the limit $\kappa \to 0$ also depends on the type of homogeneous BC at the opposing surface of the film. According to Eq. (14), for $\kappa \gg 1$ the dependence of the Casimir amplitude $\Theta_o(\kappa)$ on κ approaches the following form:

$$\begin{aligned}\Theta_o(\kappa \gg 1) &\simeq \Theta_{(o,o)} + \left(\Theta_{(+,o)} - \Theta_{(o,o)}\right)\left(1 - \frac{\alpha_o}{\kappa}\right)\\ &= -\frac{\Theta_{(+,+)}}{4}\left(1 - \alpha_o\,\kappa^{-1}\right), \qquad (58)\end{aligned}$$

where we have determined $\alpha_o = 0.857(9)$ via a least-square fit.

Whereas the behavior of the Casimir amplitude $\Theta_+(\kappa)$ for the case of a homogeneous (+) BC as calculated within MFT (Fig. 21) is similar to the one obtained from MC simulations (Fig. 5), the form of $\Theta_o(\kappa)$ for the case of a homogeneous (o) BC as obtained within MFT (Fig. 22) is qualitatively different from the one obtained from MC simulations (Fig. 6). This will be addressed in more detail in Sec. VII below.

B. Scaling function of the critical Casimir force

The reduced scaling function $\theta_+(\tau,\kappa)/|\Theta_{(+,+)}|$ [Eq. (9)] of the critical Casimir force between a chemically striped surface and a homogeneous surface with (+) BC (Fig. 1) is shown in Fig. 23 for $d = 4$ (MFT) and for various values of κ. For $\kappa \to 0$, $\theta_+(\tau,\kappa)/|\Theta_{(+,+)}|$ approaches the scaling function $\theta_{(+,o)}(\tau)/|\Theta_{(+,+)}|$, i.e., the striped surface effectively mimics a surface with homogeneous (o) BC. On the other hand, for $\kappa \to \infty$, the universal scaling function of the critical Casimir force approaches the average of the scaling functions for

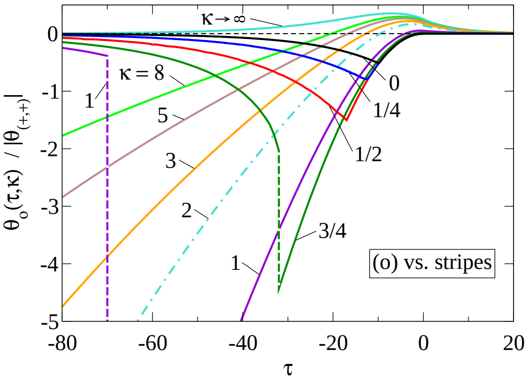

FIG. 24. Reduced universal scaling function $\theta_o(\tau,\kappa)/|\Theta_{(+,+)}|$ of the critical Casimir force for a striped surface opposite to a surface with homogeneous (o) BC (Fig. 2), as determined numerically within MFT for various values of κ. We compare the data also with the reduced scaling functions $\theta_{(o,o)}(\tau)/|\Theta_{(+,+)}|$ and $\theta_{(+,o)}(\tau)/|\Theta_{(+,+)}|$, which correspond to the limits $\kappa \to 0$ [Eq. (13)] and $\kappa \to \infty$ [Eq. (14)], respectively. For $\kappa < 2$ the numerically obtained MFT scaling functions suggest the occurrence of a cusp-like singularity or a finite jump of $\theta_o(\tau,\kappa)$ at its minimum position $\tau_{\min}$. (Due to the numerical difficulties in determining the thermodynamically stable configuration, both the positions and the depths of the minima of $\theta_o(\tau,\kappa<2)/|\Theta_{(+,+)}|$ are affected by an estimated numerical error of around 10%, which is one order of magnitude larger than for the remaining data.) For $\kappa > 2$ the scaling functions diverge for $\tau \to -\infty$ [Eq. (15)]. Compare Fig. 20 by taking into account that there, i.e., in $d = 3$, $|\Theta_{(+,+)}| = 0.820(15)$.

$(+,+)$ and $(+,-)$ BC, i.e., $\theta_+(\tau,\kappa \to \infty)/|\Theta_{(+,+)}| = (\theta_{(+,+)}(\tau) + \theta_{(+,-)}(\tau))/|2\Theta_{(+,+)}|$ [Eq. (13)]. For intermediate values of κ, the scaling functions smoothly and monotonically interpolate between these limiting cases.

As discussed in Sec. V, the behavior of the universal scaling scaling function $\theta_o(\tau,\kappa)$ for a striped surface opposite to a surface with homogeneous (o) BC (Fig. 2) is more complex than the one in the previous case. Whereas for $\tau \geq 0$ the scaling function $\theta_o(\tau,\kappa)$ smoothly interpolates between its limiting behaviors $\theta_{(o,o)}(\tau)$ for $\kappa = 0$ and $\theta_{(+,o)}(\tau)$ for $\kappa \to \infty$, for negative values of τ its dependence on κ is non-monotonic and involves a phase transition associated with the one at $\kappa = 2$ between the ground states of the system (see Eq. (55)). For $\kappa < 2$ the ground states are spatially homogeneous, which results in a vanishing value $\theta_o(\tau \to -\infty, \kappa < 2) \to 0$. The numerically obtained MFT data shown in Fig. 24 suggest that the minima of the scaling functions for $\kappa < 2$ correspond to a cusp-like singularity or even a finite jump. (Recall that θ_o is the scaling function of the critical Casimir *force*, which is the derivative of the Casimir interaction.) However, due to the presence of metastable striped and homogeneous states the numerics even within MFT is so involved that the present data suffer from an error of the position of the minimum of around 10%. Moreover, due to using the short-distance expansion in the numerical implementation of $(\pm)$ BC, it is technically difficult to distinguish these metastable states for $\kappa \simeq 2$. For $\kappa > 2$ a striped ground state is stable, which involves a divergence of the scaling function for $\tau \to -\infty$ so that for $\tau < 0$ the transition to its limiting behavior $\theta_{(+,o)}(\tau) > 0$ for $\kappa \to \infty$ is somewhat singular. Since at $T = T_c$, the critical Casimir amplitude $\Theta_o(\kappa)$ is non-negative for all values of κ (see Fig. 22; for $\kappa \lesssim 0.5$, Θ_o is vanishingly small), within MFT the scaling function $\theta_o(\tau,\kappa)$ changes sign for all values of κ at a certain value $\tau^*(\kappa) < 0$.

In the following we consider the contribution of the interface tension to the critical Casimir force for $\tau < 0$ (see Eq. (15)). Near T_c the interface tension varies as $\sigma = \sigma_0|t|^\mu$ where $\mu = (d-1)\nu$, so that $\mu = 3/2$ within MFT [65]; σ_0 is the corresponding non-universal amplitude which forms the universal amplitude ratio $\frac{1}{k_BT}\sigma_0(\xi_0^+)^{(d-1)} = R_\sigma$. Within MFT $\sigma/(k_BT_c) = 4\sqrt{2}u^{-1}(\xi_0^+)^{-(d-1)}|t|^\mu$ [70] so that $R_\sigma = \frac{2}{3}\sqrt{2}(B\xi_0^+)^2$ and $R_\sigma/|\Theta_{(+,+)}| \simeq 0.020$. For the homogeneous configuration with the interfaces parallel to the film (i.e., for $\kappa < 2$), the interface energy does not contribute explicitly to the resulting force because the area of these interfaces is not changed upon varying of the film thickness. (Note, however, that the order parameter profile across these interfaces does depend on L.) For the striped configurations, i.e., for $\kappa > 2$, in which the interfaces are oriented perpendicular to the film, the interface tension dominates the resulting force for large negative τ (i.e., L large), because approximately the interface along the z-direction has an area $L_\parallel^{d-2}L$ which is proportional to the film thickness L. Thus, the free energy Γ_s^i of such a *s*ingle *i*nterface is given by

$$\Gamma_s^i = L_\parallel^{d-2}L\sigma, \tag{59}$$

where $L_\parallel$ is the extension of the system along the invariant direction(s). For a single such interface this gives rise to a force along the normal direction:

$$F_{\Gamma,s}^i = -\frac{\partial \Gamma_s^i}{\partial L} = -L_\parallel^{d-2}\sigma. \tag{60}$$

For the striped state there are $2 \times L_\parallel/P = L_\parallel/S_+$ such interfaces so that the total force per area $L_\parallel^{d-1}$ of the film and per k_BT_c is

$$\begin{aligned}\frac{F_{\Gamma,tot}^i}{k_BT_cL_\parallel^{d-1}} &= -\frac{1}{S_+}\frac{\sigma}{k_BT_c} = -\frac{1}{L^d}\frac{1}{\kappa}L^{d-1}\frac{\sigma_0}{k_BT_c}|t|^{(d-1)\nu}\\ &= \frac{1}{L^d}\left(-\frac{1}{\kappa}R_\sigma|\tau|^\mu\right),\end{aligned} \tag{61}$$

so that its contribution $\theta_{o,\Gamma}(\tau,\kappa)$ to the universal scaling function of the critical Casimir force reads (see Eq. (9))

$$\theta_{o,\Gamma}(\tau,\kappa) = -\frac{R_\sigma}{\kappa}|\tau|^\mu, \tag{62}$$

which is attractive and becomes as strong as $\Theta_{(+,+)}$ for $|\tau|^\mu/\kappa \gtrsim 50$ within MFT. Accordingly, for the limit

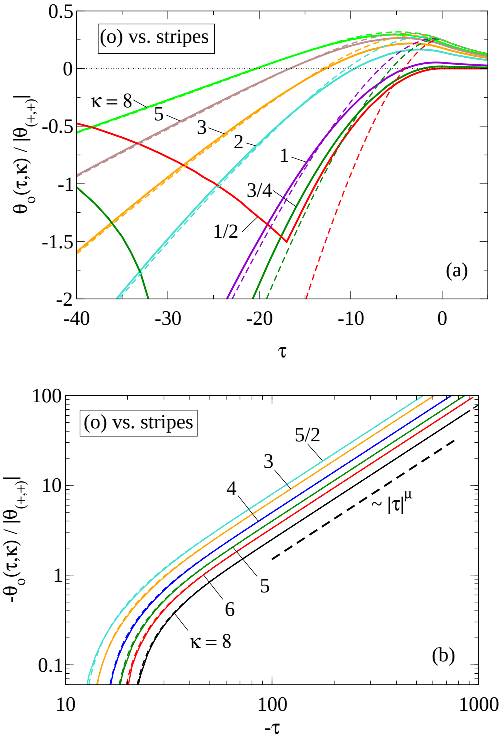

FIG. 25. Reduced universal scaling function $\theta_o(\tau,\kappa)/|\Theta_{(+,+)}|$ of the critical Casimir force for a striped surface opposite to a surface with homogeneous (o) BC (Fig. 2), as determined numerically within MFT (solid lines, same as Fig. 24). For $\tau \ll -1$ and $\kappa > 2$ they agree well with the asymptotic expression given by the r.h.s. of Eq. (15) shown as dashed lines (a). For $\kappa > 2$ and large negative values of τ, i.e., $\tau \ll -10$, the attractive interface contribution $-R_\sigma \kappa^{-1} |\tau|^\mu / |\Theta_{(+,+)}|$ [Eq. (62)] dominates the the scaling function $\theta_o(\tau,\kappa)/|\Theta_{(+,+)}|$ (b).

$\tau \ll -1$ and $\kappa > 2$ the scaling function of the critical Casimir force approaches the expression given in Eq. (15), which corresponds to the sum of the homogeneous contribution and the contribution due to the interfaces oriented perpendicular to the film surfaces.

Figure 25 compares $\theta_o(\tau,\kappa)$ for a striped surface opposite to a surface with homogeneous (o) BC as determined numerically within MFT with the estimate of the corresponding interface contribution as given in Eq. (15). The dashed lines shown in Fig. 25 correspond to Eq. (15). They are approached by the actual scaling functions shown as solid lines in Fig. 25. As expected, Eq. (15) does neither describe the behavior for $\kappa < 2$ nor the one for small absolute values of τ. However, for $\tau \ll -1$ and $\kappa > 2$, the scaling functions agree rather well with their asymptotic behavior given in Eq. (15).

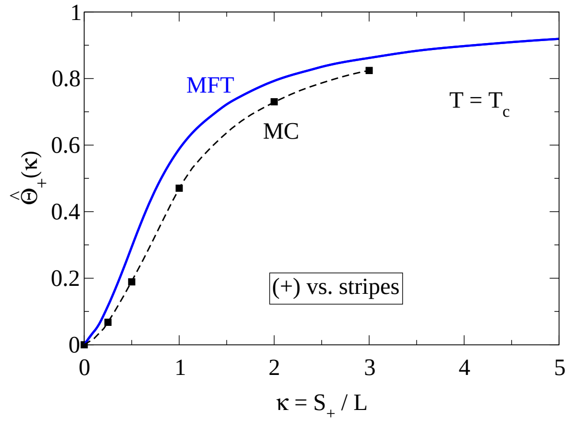

FIG. 26. Comparison of the normalized critical Casimir amplitude $\hat{\Theta}_+(\kappa) = [\Theta_+(\kappa) - \Theta_+(\kappa \to 0)]/[\Theta_+(\kappa \to \infty) - \Theta_+(\kappa \to 0)]$ [Eq. (63)] for a homogeneous (+) wall opposite to a striped wall (Fig. 1) as obtained from MC data (symbols; same as Fig. 5) and within MFT (solid line; see Fig. 21).

VII. COMPARISON BETWEEN MEAN-FIELD THEORY AND MONTE CARLO DATA

A. Critical Casimir amplitude at T_c

Different than the MC data for $d = 3$, the universal scaling functions of the critical Casimir force obtained within mean-field theory can be determined only up to an unknown constant amplitude. In order to facilitate nonetheless a valuable comparison between them, which illustrates the dependence of the scaling functions on the spatial dimension d, it is useful to normalize them by an overall amplitude so that the unknown constant amplitude for the MFT results drops out. In the previous section we normalized the various scaling functions by one and the same universal critical Casimir amplitude $|\Theta_{(+,+)}|$. Here, we propose an alternative normalization, which makes use only of that scaling function under consideration and also normalizes the ratios between the corresponding critical Casimir amplitudes, which depend on d:

$$\hat{\Theta}(\kappa) \equiv \frac{\Theta(\kappa) - \Theta(\kappa \to 0)}{\Theta(\kappa \to \infty) - \Theta(\kappa \to 0)} \to \begin{cases} 0, & \kappa \to 0, \\ 1, & \kappa \to \infty. \end{cases} \tag{63}$$

As discussed in the previous sections, the critical Casimir amplitude between a chemically striped wall and a homogeneous wall with (+) BC interpolates between $\Theta_+(\kappa \to 0) = \Theta_{(+,o)}$ and $\Theta_+(\kappa \to \infty) = (\Theta_{(+,+)} + \Theta_{(+,-)})/2$. Figure 26 shows the corresponding normalized critical Casimir amplitude $\hat{\Theta}_+(\kappa)$ [Eq. (63)] as obtained from MC data (symbols) as well as obtained within MFT (full line). As can be inferred from Fig. 26 the behavior of the normalized Casimir amplitude $\hat{\Theta}_+(\kappa)$ as a function of κ as obtained from MFT ($d = 4$) is rather similar to the one in $d = 3$. Thus, for this geometry the

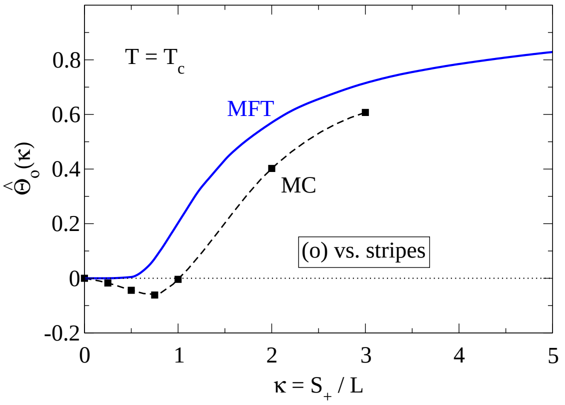

FIG. 27. Normalized Casimir amplitude $\hat{\Theta}_o(\kappa) = [\Theta_o(\kappa) - \Theta_o(\kappa \to 0)]/[\Theta_o(\kappa \to \infty) - \Theta_o(\kappa \to 0)]$ [Eq. (63)] for a homogeneous (o) wall opposite to a striped wall (Fig. 2) as obtained from MC data (symbols; same as Fig. 6) and within MFT (solid line; see Fig. 22). In contrast to the behavior shown in Fig. 26, the MFT results differ qualitatively from the behavior in $d = 3$. In both cases MFT overestimates the strength of the force (here for $\kappa \gtrsim 0.75$). $\hat{\Theta}_o(\kappa \to \infty)$ attains its limiting value 1 slower than $\hat{\Theta}_+(\kappa \to \infty)$.

effects of the chemical patterning are captured even semi-quantitatively by MFT.

In contrast, for the case of a homogeneous (o) surface opposite to a striped one (Fig. 2), we find qualitative differences. In Fig. 27 the normalized critical Casimir amplitude $\hat{\Theta}_o(\kappa)$ [Eq. (63)], as obtained both in $d = 3$ and within MFT, is shown, using the corresponding limits $\Theta_o(\kappa \to 0) = \Theta_{(o,o)}$ and $\Theta_o(\kappa \to \infty) = \Theta_{(+,o)}$. Whereas the critical Casimir amplitude as obtained from MC simulations shows a non-monotonic behavior and changes sign as a function of κ, the mean-field amplitudes are always positive and monotonically increasing as function of κ. As expected, the absence of fluctuations within MFT affects the quantitative estimate of the Casimir amplitude more strongly for the (o) BC than for the (+) BC.

B. Scaling function of the critical Casimir force

In order to compare also the temperature dependence of the scaling functions $\theta_{+/o}(\tau, \kappa)$ of the critical Casimir force in $d = 3$ with their corresponding MFT estimates, it is useful to not only normalize the amplitude of the latter but also to rescale them along the τ axis by an overall factor. Although this is an ad hoc procedure, it has turned out that a suitable combination of such rescaled MFT results with only partly available MC data might be a successful method in order to obtain quantitatively reliable approximations in an extended range of variables [71]. In the following we use a simple normalization of the MFT scaling functions $\theta^{\mathrm{MFT}}_{+/o}(\tau, \kappa)$. In Figs. 28 and 29 the mean-field scaling functions are rescaled linearly according to

$$\hat{\theta}^{\mathrm{MFT}}_{+/o}(\tau, \kappa) \equiv \frac{\theta_{+/o}(\tau_{\max,+/o}, \kappa \to \infty)}{\theta^{\mathrm{MFT}}_{+/o}(\tau^{\mathrm{MFT}}_{\max,+/o}, \kappa \to \infty)} \theta^{\mathrm{MFT}}_{+/o}\left(\frac{\tau^{\mathrm{MFT}}_{\max,+/o}}{\tau_{\max,+/o}} \tau, \kappa\right) \quad (64)$$

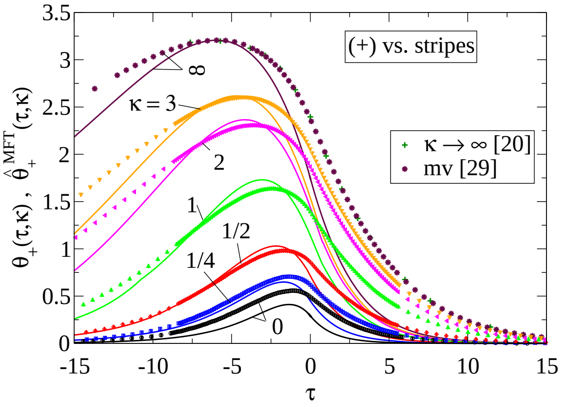

FIG. 28. Comparison of the scaling functions $\theta_+(\tau, \kappa)$ for a wall with a homogeneous (+) BC opposite to a chemically striped wall (Fig. 1) as obtained for $d = 3$ and within MFT, i.e., for $d = 4$. The symbols are the data obtained from the MC simulations shown in Fig. 13. The data obtained for $\kappa \to \infty$ [20] agree with the *mean value* of the data for (+, +) and (+, −) BC of Ref. [29]. The solid lines correspond to the MFT scaling functions $\hat{\theta}^{\mathrm{MFT}}_+$ shown in Fig. 23 which have been rescaled according to Eq. (64) (see the main text and the caption of Fig. 13). Upon construction, for $\kappa = \infty$ the positions and the heights of the maxima for $d = 3$ and $d = 4$ agree.

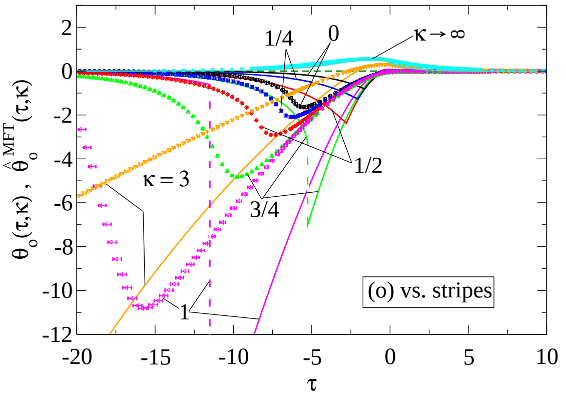

FIG. 29. Comparison of the scaling functions $\theta_o(\tau, \kappa)$ for a homogeneous (o) wall opposite to a striped wall (Fig. 2). The symbols correspond to the MC data ($d = 3$) shown in Fig. 20, whereas the solid lines correspond to the MFT scaling functions ($d = 4$) shown in Fig. 24 which have been rescaled according to Eq. (64). In contrast to Fig. 28, the rescaled MFT scaling functions differ qualitatively from the corresponding ones in $d = 3$. Upon construction, for $\kappa = \infty$ the positions and the heights of the maxima for $d = 3$ and $d = 4$ agree.

so that for $\kappa \to \infty$ the positions and the values of the maxima of the rescaled scaling functions $\hat{\theta}^{\rm MFT}_{+/o}$ agree with those of the MC data. In Eq. (64) $\tau_{{\rm max},+/o}$ and $\tau^{\rm MFT}_{{\rm max},+/o}$ correspond to the position of the maximum of the scaling functions for $\kappa \to \infty$ in $d = 3$ and $d = 4$, respectively. For the case of a homogeneous $(+)$ wall opposite to a striped wall we can infer from the data of Ref. [29] the rough estimates $\tau_{{\rm max},+} \simeq -6.0$ and $\theta_+(\tau_{{\rm max},+}, \kappa \to \infty) \simeq 3.21$ in $d = 3$ (see the caption of Fig. 13 and Refs. [20, 29]) and $\tau^{\rm MFT}_{{\rm max},+} \simeq -31.960$ and $\theta^{\rm MFT}_+(\tau^{\rm MFT}_{{\rm max},+}, \kappa \to \infty) \simeq 2.7531|\Theta_{(+,+)}|$ in $d = 4$ (by taking the mean value of the scaling functions for $(+,+)$ and $(+,-)$ BC from Ref. [21]; see Fig. 23). For a homogeneous (o) wall opposite to a striped wall one has $\tau_{{\rm max},o} = -1.174(10)$ and $\theta_o(\tau_{{\rm max},o}, \kappa \to \infty) = 0.564(3)$ in $d = 3$ (see Ref. [31] which agrees with the result shown in Fig. 7) and $\tau^{\rm MFT}_{{\rm max},o} \simeq -7.0275$ and $\theta^{\rm MFT}_o(\tau^{\rm MFT}_{{\rm max},o}, \kappa \to \infty) \simeq 0.35280|\Theta_{(+,+)}|$ in $d = 4$ as obtained from Ref. [21].

Figure 28 shows the comparison of the scaling functions of the critical Casimir force for a homogeneous $(+)$ wall opposite to a striped wall (see Fig. 1). All MFT curves have been rescaled by the same factors according to Eq. (64) so that the position and the height of the maximum of the MFT curve for $\kappa \to \infty$ agrees with the one obtained from the MC simulations in $d = 3$. As can be inferred from Fig. 28, the rescaled MFT behaviors as a function of τ show a qualitative agreement with the corresponding MC results even for finite values of κ.

In Fig. 29 we compare the scaling functions of the critical Casimir force for a homogeneous wall with (o) BC opposite to a striped one (see Fig. 2). The MFT scaling functions have been rescaled according to Eq. (64). In contrast to the case shown in Fig. 28, these rescaled MFT scaling functions for the (o) case shown in Fig. 29 differ qualitatively from the corresponding behavior in $d = 3$. Whereas for $\kappa < 2$ the MFT results suggest that the minima of the scaling functions exhibit a cusp-like singularity or a finite jump, the scaling functions $\theta_o(\tau, \kappa)$ in $d = 3$ are analytic at their minima. These differences are analogous to the ones obtained for homogeneous (o,o) BC at both surfaces [67, 68].

VIII. SUMMARY AND OUTLOOK

Within the Ising universality class we have studied the critical Casimir force for a film of thickness L by using Monte Carlo (MC) simulations in $d = 3$ spatial dimensions and by using mean-field theory. Along the lateral directions we have employed periodic *b*oundary *c*onditions (BC), whereas along the normal direction at the two confining surfaces fixed BC have been imposed. We have considered two cases: a homogeneous wall with $(+)$ BC opposite to a wall patterned with alternating chemical stripes of equal width $S_+ = S_-$ with $(+)/(-)$ BC (Fig. 1) and a homogeneous wall corresponding to (o) BC opposite to a striped wall (Fig. 2). In the limit of very narrow stripes, i.e., $\kappa \equiv S_+/L \to 0$, the striped wall effectively mimics the behavior of Dirichlet (o) BC, so that for $\kappa \to 0$ the system reduces to the homogeneous cases with $(+,o)$ or (o,o) BC, respectively (see Figs. 3 and 4). In the opposite limit $\kappa \to \infty$, i.e., very broad stripes, in the first case (+; Fig. 1) the critical Casimir force equals the mean value of the corresponding forces for films with homogeneous $(+,+)$ and $(+,-)$ boundary conditions at both surfaces, respectively. On the other hand, in the second case (o; Fig. 2), deep in the two-phase regime, the corresponding limit is singular.

We have investigated this system by combining MC simulations and numerical integration as well as by carrying out numerically the corresponding MFT calculation. We have employed an improved lattice model, for which the leading scaling corrections are suppressed. We have obtained the following main results:

- In the finite size scaling limit the critical Casimir force $F_C = L^{-d}\theta(\tau, \kappa)$ per area and in units of k_BT is described (Eq. (9)) by a universal scaling function $\theta(\tau, \kappa)$, with the scaling variables $\tau \equiv t(L/\xi_0^+)^{1/\nu}$ and $\kappa \equiv S_+/L$. Here $t \equiv (T - T_c)/T_c$ is the reduced temperature, ξ_0^+ is the non-universal amplitude of the correlation length $\xi(t \to 0^+) = \xi_0^+|t|^{-\nu}$, and S_+ is the width of the stripes on the lower surface. In the limit $\kappa \to 0$ the patterned surface attains an effective Dirichlet BC (Eq. (12)). Within the range of aspect ratios $\rho = L/L_\parallel$ (Figs. 1–4) considered here, the MC data do not display a detectable dependence on ρ. Therefore we regard our results as the ones corresponding to the extrapolation to the film limit $\rho \to 0$.

- In the limit of broad stripes, i.e., $\kappa \gg 1$, the effects of the chemical steps separating the stripes vanish as $\propto \kappa^{-1}$ (Eqs. (13) and (14)). Thus, the total critical Casimir force effectively approaches the sum of the forces between the individual stripes and the opposing wall. Accordingly, the assumption of additivity of the forces (which underlies the Derjaguin or proximity force approximation) generally holds for $\kappa \to \infty$. However, in the case of a homogeneous wall with (o) BC opposite to a chemically striped wall, for $\kappa > 2$ and $\tau \ll -1$, due to the formation of interfaces perpendicular to the film surfaces, the scaling function of the force varies as $\propto \kappa^{-1}|\tau|^\mu \propto L^d/S_+$ (for a fixed temperature $t < 0$; Eq. (15)), so that F_C does not decay for $L \to \infty$ as long as $L < S_+/2$. Accordingly, for $\tau \to -\infty$, in the subsequent limit $\kappa \to \infty$ force additivity breaks down. The two limits $\kappa \to \infty$ and $\tau \to -\infty$ do not commute.

- By using MC simulations for $d = 3$, we have determined the critical Casimir amplitude at T_c for various values of κ, in the case of the BC illustrated in Figs. 1 and 2 as well as in the limit $\kappa \to 0$, which corresponds to the BC shown in Figs. 3 and 4. The results are reported in Eqs. (34)-(37) for the case of Fig. 1 and in Eqs. (40)-(46) for the case of Fig. 2. Whereas in the first case involving a homogeneous $(+)$ wall, the critical Casimir force is always repulsive (Fig. 5), in the case of a homogeneous (o) wall the critical Casimir amplitude is nonmonotonic and changes sign as a function of κ (Fig. 6).

- Concerning $T \neq T_c$ we have determined the critical Casimir scaling functions $\theta_{+/o}(\tau, \kappa)$ in $d = 3$ for various values of κ, as well as in the limit $\kappa \to 0$. In Figs. 7–12 and 14–19 we show the scaling functions $\theta_+(\tau, \kappa)$ and $\theta_o(\tau, \kappa)$, respectively, as determined for various film thicknesses. In Fig. 13 we compare the universal scaling function $\theta_+(\tau, \kappa)$ of the critical Casimir force between a homogeneous wall with $(+)$ BC and a striped wall (Fig. 1) for various values of κ, as determined from systems with the largest film thickness considered here, i.e., $L_z = 24$, where $L_z = L/a + 1$ and a is the MC lattice constant. We also compare our results with the universal scaling function for the geometry consisting of a single chemical step (in the limit of vanishing aspect ratio studied in Ref. [20]) which corresponds to the limit $\kappa \to \infty$. In this case, within the entire range $0 \leq \kappa \leq \infty$ the critical Casimir force is always repulsive.

- In contrast, for the case of a homogeneous (o) wall opposite to a striped one (Fig. 2), the scaling function of the critical Casimir force exhibits a rather different behavior. As shown in Fig. 20, the critical Casimir force varies nonmonotonically and changes sign as a function of κ as well as a function of τ. Moreover, for $\tau < 0$ and for finite values of κ the force may become much stronger than the ones for its limiting homogeneous cases (o, o) and $(+, o)$ attained for $\kappa \to 0$ and $\kappa \to \infty$, respectively, which are also shown in Fig. 20. At $\kappa = 2$ the system exhibits a transition of ground states from homogeneous states for $\kappa < 2$ to vertically striped states for $\kappa > 2$. Whereas the scaling functions of the critical Casimir force for the homogeneous states exhibit a minimum at finite $\tau < 0$ and vanish for $\tau \to -\infty$, for $\kappa > 2$ the scaling functions diverge for $\tau \to -\infty$ as $\propto |\tau|^{\mu}$ in accordance with Eq. (15). This is confirmed by the MC results for $\kappa = 3$ as shown in Fig. 19. Thus, the scaling functions of the critical Casimir force as obtained for this case – belonging to the *Ising* bulk universality class – do not vanish for $\tau \to -\infty$. So far this peculiar feature is only known for the critical Casimir force acting in films belonging to the XY bulk universality class and thus exhibiting Goldstone modes [22–28, 68, 72].

- In Sec. VI, within MFT we have calculated the corresponding scaling functions for the critical Casimir force for the two cases sketched in Fig. 1 and Fig. 2. The results for the suitably reduced critical Casimir amplitudes are shown in Figs. 21 and 22 as a function of κ within a wide range of values. For $\kappa \gg 1$ the numerical MFT results agree with the asymptotic behaviors of the scaling functions Θ_+ and Θ_o given in Eq. (13) and Eq. (14), respectively, according to which they approach their corresponding limits for $\kappa \to \infty$ as κ^{-1}. The suitably reduced universal scaling functions for $\tau \neq 0$, as obtained within MFT, are shown in Fig. 23 for various values of κ in the case of a homogeneous surface with $(+)$ BC opposite to a striped surface. They interpolate smoothly between their limiting cases and always correspond to a repulsive critical Casimir force.

- In the case of a homogeneous surface with (o) BC opposite to a striped surface the reduced MFT scaling functions are presented in Fig. 24. They show a rich dependence on κ. For $\kappa < 2$ and $\tau < 0$ the scaling function exhibits a minimum, and our numerical data suggest a cusp-like singularity or a finite jump of the scaling function at its minimum. For $\kappa > 2$ the scaling functions diverge for $\tau \to -\infty$ and the MFT scaling functions agree to large extent with the interface estimate given by Eq. (15) (Fig. 25).

- The comparison of the suitably normalized Casimir amplitudes as obtained from MC simulations in $d = 3$ with the corresponding MFT ones reveals a good agreement for a homogeneous $(+)$ surface opposite to a striped surface (Fig. 26) but qualitative differences for the corresponding (o) case (Fig. 27). Whereas in the latter case the data for $d = 3$ show a nonmonotonic behavior and a change of sign as function of κ, in $d = 4$ the MFT Casimir amplitudes are always positive.

- Similarly, as shown in Fig. 28, the behaviors of the full scaling functions $\theta_{+/o}(\tau, \kappa)$ as obtained from simulations and within MFT plus a suitable rescaling (Eq. (64)) agree qualitatively to large extent for a homogeneous $(+)$ wall opposite to a striped one. On the other hand, for a homogeneous (o) surface opposite to a striped surface the MFT scaling functions show, even after rescaling, qualitative differences to the ones obtained via MC simulations (Fig. 29). However, within MFT as well as in $d = 3$, in the latter (o) case (Fig. 2) we always observe a change of sign of the critical Casimir force from negative values at $\tau \ll -1$ to positive values for $\tau > 0$. In $d = 3$ this occurs for $\kappa \gtrsim 3$ and within MFT for all values of $\kappa \gtrsim 0.5$. At a fixed reduced temperature t, this zero at $\tau = \tau_0$ corresponds to a *stable* distance $L_0(t) = \xi_0^+(\tau_0/t)^{\nu}$ at which the upper plate levitates above the lower plate due to critical Casimir forces alone. The levitation height $L_0(t)$ varies very sensitively as function of the reduced temperature $t = (T - T_c)/T_c$.

- The computation of the critical Casimir force requires to subtract the bulk free energy density from the free energy density of the film. This bulk quantity is independent of the BC. For $d = 3$ we have determined it using a combination of MC simulations and numerical integration (see App. B).

The present study is relevant for the critical behavior of films belonging to the Ising universality class and in the presence of a chemically structured substrate. This can be experimentally realized by considering complete wetting films of binary liquid mixtures near their critical endpoints of demixing and by exposing their vapor phases to a chemically structured substrate [10, 19]. The critical Casimir forces can be inferred by monitoring the thicknesses of the wetting films. This realizes the $(+)$ BC versus a striped surface. The surface fields describe the preferences of the two species for the confining interfaces of the wetting films.

Another realization consists of studying directly the force acting on a colloidal particle immersed in a critical binary liquid mixture and exposed to a chemically structured substrate, as has been done in Ref. [14]. In this case the *normal* critical Casimir force is approximately the one for the film geometry investigated here, provided the radius of the colloidal particle is sufficiently large relative to its distance from the wall. However, near T_c for such a system an additional *lateral* critical Casimir force sets in. In Ref. [41] the critical Casimir force for a sphere in front of a chemically structured substrate has been studied by means of mean-field theory as well as in $d = 3$ by using the Derjaguin approximation. In this study, it was found that for suitable geometric features of the stripes on the substrate and in the presence of homogeneous BC on the spherical colloid levitation is possible even for $\tau > 0$, i.e., in the homogeneous phase of the solvent. Although these experimental studies [14, 15] are closely related to the setup studied here, a re-evaluation of the existing data is not sufficient in order to compare them with the present theoretical predictions. On one hand, the authors of Refs. [14, 15] have measured only the *lateral* forces acting on the colloidal particles, and not the *normal* ones studied here. On the other hand, in order to effectively mimic the film geometry studied here, the radius of the colloidal particles should be much larger than the stripe widths S_+ and S_-, whereas the length scales realized in those experimental studies are of the same size [14, 15].

In view of recent MC results for the critical Casimir force of a sphere in front of a homogeneous wall [34], it would be very interesting to extend this study by considering a sphere in front of a chemically structured wall. Besides analyzing directly the latter experimental setup, this would also provide the possibility of elucidating the range of validity of the Derjaguin approximation, which is commonly employed for curved geometries [40, 41].

Here we have determined the critical Casimir force in the presence of a chemically structured substrate by using MC simulations in spatial dimension $d = 3$, and by using mean-field theory, which holds in $d = 4$. In order to complement this spatial dependence and to further probe the relevance of fluctuations, it would be interesting to investigate the corresponding system in $d = 2$, where some exact results are available [43] and conformal invariance allows one to determine exactly certain critical properties.

The present study also lends itself to further extensions. Here we have considered stripes with $(+)$ and $(-)$ BC of equal widths. A natural extension of the present study would consist of calculating the critical Casimir force as a function of the ratio of the widths of the $(+)$ and $(-)$ stripes. Moreover, by considering two striped surfaces, one can also investigate the corresponding lateral critical Casimir force. So far the case of two striped surfaces has been investigated by mean-field theory for the film geometry [38]; the issue of the lateral force has been analyzed by mean-field theory and in $d = 3$ within the Derjaguin approximation for the sphere-wall geometry [41].

Finally, as mentioned in Secs. V-VI, for the BC shown in Fig. 2 and for $\kappa = 2$ the system displays a rich glassy behavior at low temperatures. This deserves further investigations.

ACKNOWLEGDEMENTS

We are grateful to Svyatoslav Kondrat and Thomas F. Mohry for useful discussions and thank Martin Hasenbusch and Oleg Vasilyev for providing MC data for the homogeneous cases.

Appendix A: Monte Carlo simulations

In this appendix we report certain technical details of the MC simulations we have performed. As explained in Sec. IV, the evaluation of the Casimir force at T_c has been carried out in two steps. First, we have determined the thermal average $\langle \mathcal{H}_2 - \mathcal{H}_1 \rangle_\lambda$ which appears in Eq. (28). This is obtained by a standard MC simulation for the ensemble characterized by the crossover Hamiltonian $\mathcal{H}_\lambda$ defined in Eq. (25). We have implemented a combination of the standard Metropolis and Wolff cluster algorithms: each MC step consists of 1 Metropolis sweep over the entire lattice in lexicographic order and L_z Wolff single-cluster flips; L_z denotes the total number of lattice layers including the surfaces of fixed spins, so that there are $L_z - 2$ layers of fluctuating spins in the case of the BC shown in Fig. 1, $L_z - 1$ layers in the case of BC shown in Figs. 2 and 3, and L_z layers in the case of the (o, o) BC illustrated in Fig. 4. As random number generator we have used the double precision SIMD-oriented Fast Mersenne Twister (dSFMT) [73]. Important details of the simulations performed at the critical temperature are reported in Tables V-IX. Additional details concerning the implementation of the simulating algorithm can be found in Ref. [20].

As explained in Sec. V, the determination of the scaling function for the critical Casimir force has been obtained by sampling the reduced energy densities $E(\beta', L_z, L_x, s_+)$ and $E(\beta', L_z-1, L_x, s_+)$ (see Eq. (54)) followed by carrying out numerically the integration in Eq. (54) by using Simpson's rule. An upper bound of the systematic error due to the discretization of the integrals can be determined by sampling the fourth derivative of the integrand: by computing $\partial^4 E(\beta, L_z, L_x, s_+)/(\partial\beta^4)$ we have checked that such a systematic error is always negligible compared to the statistical errors. (Since for $L_z \to \infty$ the quantity $\partial^4 E(\beta, L_z, L_x, s_+)/(\partial\beta^4)$ diverges at the critical point, the number of sampled points has to increase with L_z.) In Table X we report important details concerning these simulations associated with Eq. (54). For each film thickness and BC we have considered the same three aspect ratios ρ for determining the scaling functions as the ones used for determining the critical Casimir amplitude (see Tables V-IX). For the BC shown in Figs. 1 and 3, we have verified that the sampled reduced energy densities are de facto independent of ρ. Therefore our results capture reliably the limit $\rho \to 0$; we have averaged them over the three aspect ratios considered. Concerning the BC shown in Figs. 2 and 4, as discussed in Sec. V, the data exhibit a weak dependence on the aspect ratio at low temperatures and we have considered the three aspect ratios separately, i.e., without taking this average.

Finally, we mention that with the above described simulation algorithm and for the BC shown in Fig 2, we occasionally observed the appearance of metastable states at low temperatures, which cause the thermalization of the run to be rather long. We have found that this problem can be healed by starting the simulations with an ordered states.

Appendix B: Determination of the bulk free energy density

Here we report certain details concerning the determination of the bulk free energy density which is needed for calculating the critical Casimir force (see Eqs. (50) and (53)). For this purpose we have simulated the improved Blume-Capel model described by Eq. (16) for a simple cubic lattice with periodic BC in all directions and lattice sizes $L_z = 24 - 256$. For this system we have determined the reduced energy density $E(\beta, L_z)$ and the reduced free energy density $F(\beta, L_z)$ as defined in Eqs. (20) and (21). For the sake of simplicity, here we omit the dependence on L_x and s_+ because the lattice considered here has the same size in all directions and it does not have any surface. Since the aim is to extract the thermodynamic limit of these quantities from finite-size results, we recall the expected behavior of the corresponding finite-size parts. For $T \neq T_c$ and $L_z \gg \xi$, $E(\beta, L_z)$ approaches its infinite-volume limit $E_{\text{bulk}}(\beta)$ as

$$\delta E(\beta, L_z) \equiv E(\beta, L_z) - E_{\text{bulk}}(\beta) \sim (L_z/\xi)^{k+1}\, e^{-L_z/\xi}, \tag{B1}$$

where k is an integer. Conversely, in the region where $\xi \approx L_z$, one has ($\alpha = 2 - 3\nu$)

$$\delta E(\beta, L_z) = t^{1-\alpha}\tilde{h}_E\left(L_z/\xi\right) = \frac{1}{L_z^{3-1/\nu}} h_E\left(L_z/\xi\right), \tag{B2}$$

where the scaling function $h_E(x)$ is universal up to a prefactor and $h_E(x) = O(1)$ for $\xi \approx L_z$. The reduced free energy density $F(\beta, L_z)$ can be obtained by integrating $E(\beta, L_z)$ according to Eq. (22). It follows that, for $T > T_c$ and $L_z \gg \xi$, $F(\beta, L_z)$ approaches its infinite-volume limit $F_{\text{bulk}}(\beta)$ as

$$\delta F(\beta, L_z) \equiv F(\beta, L_z) - F_{\text{bulk}}(\beta) \sim (L_z/\xi)^{k}\, e^{-L_z/\xi}. \tag{B3}$$

In deriving Eq. (B3), we have used the fact that for $T > T_c$ the condition $L_z \gg \xi$ is satisfied throughout the interval of integration on the r.h.s. of Eq. (22). This is not the case if $T < T_c$. For $T < T_c$, $L_z \gg \xi$, and by using Eq. (22), the finite-size correction $\delta F(\beta, L_z)$ can be expressed as

$$\begin{aligned} \delta F(\beta, L_z) &\equiv F(\beta, L_z) - F_{\text{bulk}}(\beta) \\ &= \delta F(\beta \to \infty, L_z) + \int_{\infty}^{\beta} d\beta' \delta E(\beta', L_z). \end{aligned} \tag{B4}$$

In the second term of the r.h.s. of Eq. (B4) one has $L_z \gg \xi$ throughout the integration interval. Thus, by using Eq. (B1), the integral on the r.h.s. of Eq. (B4) varies as $(L_z/\xi)^k\, e^{-L_z/\xi}$. The finite-size correction $\delta F(\beta \to \infty, L_z)$ can be inferred from computing $F(\beta, L_z)$ for $\beta \to \infty$ and for a finite size L_z. For $\beta \to \infty$, the Gibbs measure is dominated by the twofold degenerate ground state, consisting of a configuration in which all spins are fixed to $+1$ or to -1. By using the definition of $F(\beta, L_z)$ given in Eq. (21), one has

$$\begin{aligned} F(\beta \to \infty, L_z) &= \frac{1}{L_z^3} \ln\left[\frac{2e^{(3\beta - D)L_z^3}}{(1+2e^{-D})^{L_z^3}}\right] \\ &= \frac{\ln 2}{L_z^3} + \ln\left(\frac{e^{3\beta - D}}{1+2e^{-D}}\right), \end{aligned} \tag{B5}$$

where D is the coupling constant appearing in the second term of the Hamiltonian given in Eq. (16). By taking the $L_z \to \infty$ in Eq. (B5), we identify the second term on the r.h.s. of Eq. (B5) as the infinite-volume limit $F_{\text{bulk}}(\beta)$ [74]. Thus we infer $\delta F(\beta \to \infty, L_z) = (\ln 2)/(L_z^3)$. Thus, for $T < T_c$ and $L_z \gg \xi$, $F(\beta, L_z)$ approaches its infinite-volume limit $F_{\text{bulk}}(\beta)$ as

$$\delta F(\beta, L_z) \sim (L_z/\xi)^{k}\, e^{-L_z/\xi} + \frac{\ln 2}{L_z^3}. \tag{B6}$$

From Eqs. (22) and (B6) one finds that

$$\int_0^{\infty} \delta E(\beta', L_z) d\beta' = \frac{\ln 2}{L_z^3}, \tag{B7}$$

$\kappa \to 0: (+,o)$				$\kappa = 1/4$				$\kappa = 1/2$			
L_z	ρ	$N_{\mathrm{steps}}/10^3$	$N_{\mathrm{therm}}/10^3$	L_z	ρ	$N_{\mathrm{steps}}/10^3$	$N_{\mathrm{therm}}/10^3$	L_z	ρ	$N_{\mathrm{steps}}/10^3$	$N_{\mathrm{therm}}/10^3$
24	1/8	1200	200	24	1/8	500	100	24	1/8	400	80
24	1/12	800	100	24	1/12	200	40	24	1/12	160	32
24	1/16	600	100	24	1/16	100	20	24	1/16	100	20
32	1/8	3000	500	32	1/8	1500	300	32	1/8	1200	240
32	1/12	1400	200	32	1/12	700	140	32	1/12	500	100
32	1/16	800	100	32	1/16	350	70	32	1/16	250	50
48	1/8	1500	200	48	1/8	1500	200	48	1/8	1500	200
48	1/12	700	100	48	1/12	700	100	48	1/12	700	100
48	1/16	350	50	48	1/16	350	50	48	1/16	350	50

TABLE V. The total number N_{steps} of MC steps and the number N_{therm} of MC steps discarded in order to achieve thermalization as used to determine the critical Casimir amplitudes for film thicknesses $L_z \geq 24$, for aspect ratios $\rho = L_z/L_x \leq 1/8$, and for the BC shown in Figs. 1 and 3. Every MC step consists of 1 Metropolis sweep over the entire lattice and L_z Wolff single-cluster flips. Additional details concerning the simulation algorithm can be found in Ref. [20].

$\kappa = 1$				$\kappa = 2$				$\kappa = 3$			
L_z	ρ	$N_{\mathrm{steps}}/10^3$	$N_{\mathrm{therm}}/10^3$	L_z	ρ	$N_{\mathrm{steps}}/10^3$	$N_{\mathrm{therm}}/10^3$	L_z	ρ	$N_{\mathrm{steps}}/10^3$	$N_{\mathrm{therm}}/10^3$
24	1/8	1600	320	24	1/8	1600	320	24	1/12	800	160
24	1/12	1100	220	24	1/12	1100	220	24	1/18	550	110
24	1/16	800	160	24	1/16	800	160	24	1/24	400	80
32	1/8	2600	520	32	1/8	2600	520	32	1/12	1300	260
32	1/12	1700	200	32	1/12	1700	340	32	1/18	850	170
32	1/16	1300	250	32	1/16	1300	200	32	1/24	650	130
48	1/8	1500	200	48	1/8	1500	300	48	1/12	750	150
48	1/12	700	100	48	1/12	700	140	48	1/18	350	70
48	1/16	350	50	48	1/16	350	50	48	1/24	170	34

TABLE VI. Same as Table V for $\kappa = 1$, 2, 3.

$\kappa \to 0: (o,o)$				$\kappa = 1/4$				$\kappa = 1/2$			
L_z	ρ	$N_{\mathrm{steps}}/10^3$	$N_{\mathrm{therm}}/10^3$	L_z	ρ	$N_{\mathrm{steps}}/10^3$	$N_{\mathrm{therm}}/10^3$	L_z	ρ	$N_{\mathrm{steps}}/10^3$	$N_{\mathrm{therm}}/10^3$
24	1/8	12000	1200	24	1/8	12000	1200	24	1/8	12000	1200
24	1/12	8000	800	24	1/12	8000	800	24	1/12	8000	800
24	1/16	6000	600	24	1/16	6000	600	24	1/16	6000	600
32	1/8	32000	600	32	1/8	6000	600	32	1/8	6000	600
32	1/12	16000	300	32	1/12	3000	300	32	1/12	3000	300
32	1/16	8000	150	32	1/16	1500	150	32	1/16	1500	150

TABLE VII. Same as Table V for the BC of Figs. 2 and 4.

$\kappa = 3/4$				$\kappa = 1$			
L_z	ρ	$N_{\mathrm{steps}}/10^3$	$N_{\mathrm{therm}}/10^3$	L_z	ρ	$N_{\mathrm{steps}}/10^3$	$N_{\mathrm{therm}}/10^3$
24	1/9	12000	120	24	1/8	12000	1200
24	1/12	8000	800	24	1/12	8000	800
24	1/15	6000	600	24	1/16	6000	600
32	1/9	6000	600	32	1/8	6000	600
32	1/12	3000	300	32	1/12	3000	300
32	1/15	1500	150	32	1/16	1500	150

TABLE VIII. Same as Table VII for $\kappa = 3/4$ and 1.

$\kappa=2$				$\kappa=3$			
L_z	ρ	$N_{\rm steps}/10^3$	$N_{\rm therm}/10^3$	L_z	ρ	$N_{\rm steps}/10^3$	$N_{\rm therm}/10^3$
24	1/24	600	100	24	1/24	600	60
24	1/36	400	80	24	1/36	400	60
24	1/48	300	60	24	1/48	300	60
32	1/24	150	30	32	1/24	150	20
32	1/36	70	15	32	1/36	70	10
32	1/48	40	8	32	1/48	40	8

TABLE IX. Same as Table VII for $\kappa = 2$ and 3.

L_z	β_0	$\beta_{\rm max}$	$\Delta\beta$
8	0.327721735	0.427721735	0.0005
12	0.327721735	0.427721735	0.0001
16	0.327721735	0.427721735	0.0005
24	0.377721735	0.397721735	0.00002

TABLE X. The lowest (β_0) and the highest ($\beta_{\rm max}$) inverse temperatures used for the computation of the scaling functions associated with the free energy differences via Eq. (54). The integrals have been computed numerically using Simpson's rule, with the reported intervals $\Delta\beta$ between two consecutive points. For each film thickness we have considered the same three aspect ratios as the ones used for determining the critical Casimir amplitude (see Tables V-IX).

L	$\beta_{\rm min}$	$\beta_{\rm max}$	$\Delta\beta$
24	0.327721735	0.427721735	0.0002
32	0.347721735	0.427721735	0.0001
48	0.367721735	0.407721735	0.0001
64	0.377721735	0.397721735	0.0001
96	0.380521735	0.395721735	0.00005
128	0.381521735	0.394521735	0.00005
192	0.384121735	0.393321735	0.00002
256	0.385321735	0.391321735	0.00001

TABLE XI. The interval of integration $[\beta_{\rm min}, \beta_{\rm max}]$ for each lattice size L used in the determination of the bulk free energy density. We have implemented Simpson's rule with the reported distances $\Delta\beta$ between two consecutive points.

where the support of the integrand is actually confined to the region where $L_z \approx \xi$. In this region the finite size correction of the reduced free energy density is given by

$$\delta F(\beta, L_z) = \frac{1}{L_z^3} h_F\left(L_z/\xi\right), \qquad \text{(B8)}$$

where, as in Eq. (B2), the universal scaling function $h_F(x) = O(1)$ for $\xi \approx L_z$. A comparison of the finite-size corrections for the reduced energy density given in Eqs. (B1)-(B2) and those for the reduced free energy density in Eqs. (B3), (B6), and (B7) shows that $F(\beta, L_z)$ converges faster to limit for $L_z \to \infty$ than $E(\beta, L_z)$. The only exception to this rule occurs in the low-temperature phase, $T < T_c$ and $L_z \gg \xi$, where the reduced free energy density exhibits an additional finite-size correction $\ln 2/L^3$ (see Eq. (B7)). However, because this correction term is known exactly, one can eliminate it by subtracting it explicitly.

In order to compute the bulk free energy density, we proceed as follows. At a given lattice size L_z, we compute the reduced energy density $E(\beta, L_z)$ in an interval $[\beta_{\rm min}, \beta_{\rm max}]$ around the inverse critical temperature $\beta_c = 0.387721735(25)$ [45]. In order to minimize the error bars we have implemented the control-variates scheme introduced in Ref. [75]. Control variates are observables which have a vanishing mean value and therefore can be added to any observable without changing its mean value; control variates provide also an additional check of the MC simulations. In the second step $F(\beta, L_z) - F(\beta_{\rm min}, L_z)$ is calculated by numerically integrating Eq. (22). For this purpose we have used Simpson's rule. The resulting quantity $F(\beta, L_z) - F(\beta_{\rm min}, L_Z)$ suffers from two types of errors: a statistical error originating from the statistical error bars of the integrand $E(\beta, L_z)$ and a systematic error due to the chosen quadrature. In the present case and as mentioned above, the maximum systematic error in Simpson's rule can be computed by estimating the fourth derivative of $E(\beta, L_z)$. We have always checked that such an error is at least one order of magnitude smaller than the statistical error, so that it can be safely neglected and the statistical error bar is a correct measure of the uncertainty of the reduced free energy density. The integration of $E(\beta, L_z)$ leads to the value of $F(\beta, L_z) - F(\beta_{\rm min}, L_z)$ for several inverse temperatures $\beta \in [\beta_{\rm min}, \beta_{\rm max}]$. For those values of $\beta < \beta_c$ for which $L_z \gg \xi$, we regard our results for finite L_z to be the ones for infinite L_z if the statistical error bars are smaller than the finite-size correction. To this end, we have checked that $E(\beta, L_z)$ is, within the numerical accuracy, independent of L_z by comparing the values obtained for two consecutive lattice sizes: as discussed above, $E(\beta, L_z)$ is expected to converge to the thermodynamic limit slower than $F(\beta, L_z)$. Roughly speaking, with the present numerical accuracy, the finite-size scaling corrections are negligible for $L_z/\xi \le 20$. For $T < T_c$ we use the more conservative bound $L_z/\xi \le 35-40$, and we explicitly subtract the additional finite-size term $(\ln 2)/L_z^3$ which appears in Eq. (B7). We note that the non-universal amplitude ξ_{0l}^{-} of the correlation length below T_c is roughly half of ξ_{0l}^{+}: $\xi_{0l}^{+}/\xi_{0l}^{-} = 1.957(7)$ [76]. At any given lattice size L_z, this procedure results in the estimate of the bulk free energy density for a subset $[\beta_{\rm min}, \beta_{\rm inf}] \cup [\beta_{\rm sup}, \beta_{\rm max}]$ of the integration interval $[\beta_{\rm min}, \beta_{\rm max}]$, with $\xi(\beta_{\rm inf}) \approx L_z/20$ and $\xi(\beta_{\rm sup}) \approx L_z/40$. Thus, for $\beta \leq \beta_{\rm inf}$ and $\beta \geq \beta_{\rm sup}$, $F(\beta, L_z) - F(\beta_{\rm min}, L_z)$ agrees within error bars with $F_{\rm bulk}(\beta) - F_{\rm bulk}(\beta_{\rm min})$, while $[\beta_{\rm inf}, \beta_{\rm sup}]$ is the interval in which the finite-size correction $\delta F(\beta, L_z)$ is not negligible. In the next step we have applied the above procedure for a larger lattice size $L_z' > L_z$ and the smaller integration interval $[\beta_{\rm min}' = \beta_{\rm inf}, \beta_{\rm max}' = \beta_{\rm sup}]$. This results in the quantity $F(\beta, L_z') - F(\beta_{\rm min}', L_z')$ to which we add $F(\beta_{\rm min}', L_z) - F(\beta_{\rm min}, L_z) \simeq F_{\rm bulk}(\beta_{\rm min}') - F_{\rm bulk}(\beta_{\rm min})$ as determined from the lattice size L_z, so that we finally obtain the desired quantity $F(\beta, L_z') - F_{\rm bulk}(\beta_{\rm min})$. As before, this results in the estimate of the bulk free energy for $\beta \in [\beta_{\rm min}, \beta_{\rm inf}'] \cup [\beta_{\rm sup}', \beta_{\rm max}]$, with $\beta_{\rm inf}' > \beta_{\rm inf}$ and $\beta_{\rm sup}' < \beta_{\rm sup}$. By iterating the procedure with increasing values of L_z, we progressively narrow the interval around β_c where $\xi \approx L_z$ and finite-size scaling corrections are not negligible. In Table XI we report the interval used for each lattice size considered here. The final statistical error bars for $F_{\rm bulk}(\beta)$ are generally between 4×10^{-8} and 10^{-7}. Even for the largest lattice size $L_z = 256$ we have considered, there exists of course an interval around β_c for which the condition $L_z \gg \xi$ cannot be satisfied. In such a region the finite-size scaling corrections are given by Eq. (B8). In order to ensure that the residual finite-size correction is less than the statistical error bars, we have checked that the results for $L_z = 192$ and $L_z = 256$ differ at most by one error bar. As an additional check, using Eq. (B8) and the results of Ref. [77], we can infer that the finite-size correction term is at most $\approx 0.7/(256^3) = 4 \times 10^{-8}$. For the same interval the statistical error bar is between 8×10^{-8} and 10^{-7}. Thus we conclude that our determination of the bulk free energy density is reliable within the statistical error bars.

---

[1] M. E. Fisher and P. G. de Gennes, C. R. Acad. Sci. Paris Ser. B **287**, 207 (1978).

[2] H. B. Casimir, Proc. K. Ned. Akad. Wet. **51**, 793 (1948)

[3] A. Gambassi, J. Phys.: Conf. Ser. **161**, 012037 (2009).

[4] K. Binder, in *Phase Transitions and Critical Phenomena*, edited by C. Domb and J. L. Lebowitz, Vol. 8 (Academic, London, 1983), p. 1.

[5] H. W. Diehl, in *Phase Transitions and Critical Phenomena*, edited by by C. Domb and J. L. Lebowitz, Vol. 10 (Academic, London, 1986), p. 75.

[6] M. Krech, *The Casimir Effect in Critical Systems* (World Scientific, Singapore, 1994).

[7] M. Krech, J. Phys. : Condens. Matter **11**, R391 (1999).

[8] J. G. Brankov, D. M. Dantchev, and N. S. Tonchev, *Theory of Critical Phenomena in Finite-Size Systems: Scaling and Quantum Effects* (World Scientific, Singapore, 2000).

[9] R. Garcia and M. H. W. Chan, Phys. Rev. Lett. **83**, 1187 (1999);
A. Ganshin, S. Scheidemantel, R. Garcia, and M. H. W. Chan, Phys. Rev. Lett. **97**, 075301 (2006).

[10] M. Fukuto, Y. F. Yano, and P. S. Pershan, Phys. Rev. Lett. **94**, 135702 (2005); S. Rafaï, D. Bonn, and J. Meunier, Physica A **386**, 31 (2007).

[11] R. Garcia and M. H. W. Chan, Phys. Rev. Lett. **88**, 086101 (2002);
T. Ueno, S. Balibar, T. Mizusaki, F. Caupin, and E. Rolley, Phys. Rev. Lett. **90**, 116102 (2003).

[12] C. Hertlein, L. Helden, A. Gambassi, S. Dietrich, and C. Bechinger, Nature **451**, 172 (2008).

[13] A. Gambassi, A. Maciołek, C. Hertlein, U. Nellen, L. Helden, C. Bechinger, and S. Dietrich, Phys. Rev. E **80**, 061143 (2009).

[14] F. Soyka, O. Zvyagolskaya, C. Hertlein, L. Helden, and C. Bechinger, Phys. Rev. Lett. **101**, 208301 (2008).

[15] M. Tröndle, O. Zvyagolskaya, A. Gambassi, D. Vogt, L. Harnau, C. Bechinger, and S. Dietrich, Mol. Phys. **109**, 1169 (2011).

[16] U. Nellen, L. Helden, and C. Bechinger, EPL **88**, 26001 (2009).

[17] U. Nellen, J. Dietrich, L. Helden, S. Chodankar, K. Nygård, J. F. van der Veen, and C. Bechinger, Soft Matter **7**, 5360 (2011).

[18] M. P. Nightingale and J. O. Indekeu, Phys. Rev. B **32**, 3364 (1985).

[19] M. Krech and S. Dietrich, Phys. Rev. A **46**, 1922 (1992).

[20] F. Parisen Toldin and S. Dietrich, J. Stat. Mech. P11003 (2010).

[21] M. Krech, Phys. Rev. E **56**, 1642 (1997).

[22] D. Dantchev and M. Krech, Phys. Rev. E **69**, 046119 (2004).

[23] A. Hucht, Phys. Rev. Lett. **99**, 185301 (2007).

[24] O. Vasilyev, A. Gambassi, A. Maciołek, and S. Dietrich, EPL **80**, 60009 (2007).

[25] O. Vasilyev, A. Gambassi, A. Maciołek, and S. Dietrich, Phys. Rev. E **79**, 041142 (2009); *ibid* **80** 039902(E) (2009).

[26] M. Hasenbusch, J. Stat. Mech. P07031 (2009).

[27] M. Hasenbusch, Phys. Rev. B **81**, 165412 (2010).

[28] M. Hasenbusch, Phys. Rev. E **80**, 061120 (2009).

[29] M. Hasenbusch, Phys. Rev. B **82**, 104425 (2010).

[30] A. Hucht, D. Grüneberg, and F. M. Schmidt, Phys. Rev. E **83**, 051101 (2011).

[31] M. Hasenbusch, Phys. Rev. B **83**, 134425 (2011).

[32] O. Vasilyev, A. Maciołek, and S. Dietrich, Phys. Rev. E **84**, 041605 (2011).

[33] M. Hasenbusch, Phys. Rev. B **85**, 174421 (2012).

[34] M. Hasenbusch, Phys. Rev. E **87**, 022130 (2013).

[35] A. W. Rodriguez, F. Capasso, and S. G. Johnson, Nature Photonics **5**, 211 (2011); J Lussange, R. Guérout, and A. Lambrecht, Phys. Rev. A **86**, 062502 (2012).

[36] M. Tröndle, L. Harnau, and S. Dietrich, J. Chem. Phys.

129, 124716 (2008).

[37] A. Gambassi and S. Dietrich, Soft Matter **7**, 1247 (2011).

[38] M. Sprenger, F. Schlesener, and S. Dietrich, J. Chem. Phys. **124**, 134703 (2006).

[39] F. Karimi Pour Haddadan, F. Schlesener, and S. Dietrich, Phys. Rev. E **70**, 041701 (2004); F. Karimi Pour Haddadan, and S. Dietrich, Phys. Rev. E **73**, 051708 (2006).

[40] M. Tröndle, S. Kondrat, A. Gambassi, L. Harnau, and S. Dietrich, EPL **88**, 40004 (2009).

[41] M. Tröndle, S. Kondrat, A. Gambassi, L. Harnau, and S. Dietrich, J. Chem. Phys. **133**, 074702 (2010).

[42] T. F. Mohry, A. Maciołek, and S. Dietrich, Phys. Rev. E **81**, 061117 (2010).

[43] D. B. Abraham and A. Maciołek, Phys. Rev. Lett. **105**, 055701 (2010).

[44] Z. Borjan, EPL **99**, 56004 (2012).

[45] M. Hasenbusch, Phys. Rev. B **82**, 174433 (2010).

[46] A. Pelissetto and E. Vicari, Phys. Rep. **368**, 549 (2002).

[47] F. J. Wegner, in *Phase Transitions and Critical Phenomena*, edited by C. Domb and M. S. Green, Vol. 6 (Academic, London, 1976), p. 7.

[48] M. Blume, Phys. Rev. **141**, 517 (1966).

[49] H. W. Capel, Physica **32**, 966 (1966).

[50] M. Hasenbusch, Int. J. Mod. Phys. C **12**, 911 (2001).

[51] M. Deserno, Phys. Rev. E **56**, 5204 (1997).

[52] J. R. Heringa and H. W. J. Blöte, Phys. Rev. E **57**, 4976 (1998).

[53] Y. Deng and H. W. J. Blöte, Phys. Rev. E **70**, 046111 (2004).

[54] K. E. Newmani and E. K. Riedel, Phys. Rev. B **30**, 6615 (1984).

[55] C. Bervillier, A. Jüttner, and D. F. Litim, Nucl. Phys B **783**, 213 (2007)

[56] A. Aharony and M. E. Fisher, Phys. Rev. B **27**, 4394 (1983).

[57] T. W. Capehart and M. E. Fisher, Phys. Rev. B **13**, 5021 (1976).

[58] M. Hasenbusch, J. Stat. Mech. P02005 (2009).

[59] M. Hasenbusch, J. Stat. Mech. P10006 (2009).

[60] The free energy F(λ) in units of k_BT differs from the reduced free energy density $F(\beta, L_z, L_x, s_+)$ defined in Eq. (21).

[61] W. H. Press, S. A. Teukolsky, W. T. Vetterling, and B. P. Flannery, *Numerical Recipes: The Art of Scientific Computing*, 2nd edition (Cambridge University Press, New York, 1992), chapter 15.

[62] D. J. Amit and V. Martín-Mayor, *Field Theory, the Renormalization Group, and Critical Phenomena*, 3rd edition (World Scientific, Singapore, 2005).

[63] Due to a different convention, the value $L_s = 1.42(2)$ of the extrapolation length reported in Eq. (58) of Ref. [31] is related to $c\,'_{(+,o)}$ via $L_s = 1 + c\,'_{(+,o)}$.

[64] The error bars shown in Figs. 14-19 are the sum of the statistical error bars originating from the MC sampling and the uncertainty in the determination of $c\,'$, the latter one being the dominant contribution to the error bars. The dependence on ρ is more clearly seen in the raw MC data.

[65] S.-Y. Zinn and M. E. Fisher, Physica A **226**, 168 (1996); M. E. Fisher and S.-Y. Zinn, J. Phys. A **31**, L629 (1998).

[66] H. W. Diehl, Int. J. Mod. Phys. B **11**, 3503 (1997).

[67] A. Gambassi and S. Dietrich, J. Stat. Phys. **123**, 929 (2006).

[68] R. Zandi, A. Shackell, J. Rudnick, M. Kardar, and L. P. Chayes, Phys. Rev. E **76**, 030601 (2007); A. Maciołek, A. Gambassi, and S. Dietrich, Phys. Rev. E **76**, 031124 (2007).

[69] There is a misprint in Eq. (27) of Ref. [25], where the argument of the function on the r.h.s. should be $-x/2$ instead of $-2x$. Additionally, in footnote [49] of Ref. [25], the estimate of the position of the maximum of the scaling function for a film with $(+,-)$ BC should read $\simeq -28.1$ instead of $\simeq 28.1$.

[70] E. Brézin and S. Feng, Phys. Rev. B **29**, 472 (1984).

[71] T. F. Mohry, A. Maciołek, and S. Dietrich, J. Chem. Phys. **136**, 224902 (2012).

[72] R. Zandi, J. Rudnick, and M. Kardar, Phys. Rev. Lett. **93**, 155302 (2004); V. Dohm, Phys. Rev. Lett. **110**, 107207 (2013).

[73] M. Saito and M. Matsumoto, in *Monte Carlo and Quasi-Monte Carlo Methods 2006*, ed. by A. Keller, S. Heinrich, and H. Niederreiter (Springer, Berlin, 2008) p. 607; M. Saito, PhD Thesis, Dept. of Math., Graduate School of Science, Hiroshima University, Advisor: M. Matsumoto (2007); the code and the documentation can be downloaded at `http://www.math.sci.hiroshima-u.ac.jp/∼m-mat/MT/SFMT/index.html`.

[74] We note that $F_{\rm bulk}(\beta \to \infty) \to \infty$. This holds because $F_{\rm bulk}(\beta)$ is the bulk free energy per volume and in units of $-k_BT$. The free energy per volume $-\beta F_{\rm bulk}(\beta)$ has instead a finite limit for $\beta \to \infty$.

[75] L. A. Fernandez and V. Martin-Mayor, Phys. Rev. E **79**, 051109 (2009).

[76] M. Campostrini, A. Pelissetto, P. Rossi, and E. Vicari, Phys. Rev. E **65**, 066127 (2002).

[77] V. Dohm, Phys. Rev. E **84**, 021108 (2011).